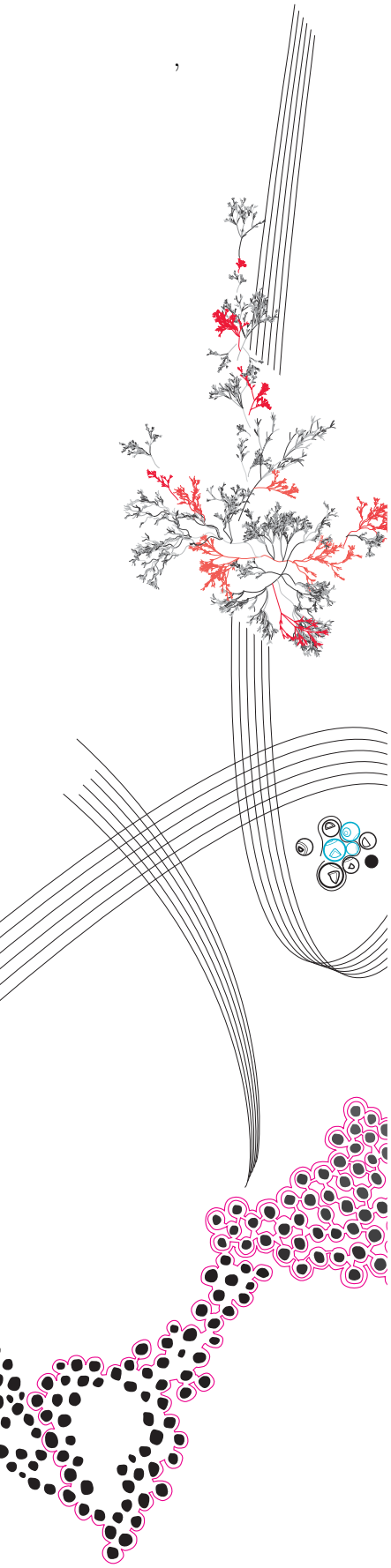

MSc Biomedical engineering
Thesis

Computational models to investigate the effect of weak electric fields on the (de)synchronization of neurons

Maud Bosman

Supervisor: Dr.ir. B.C. Schwab (chair of the committee)
Second supervisor: N. Doorn
External member: dr. H.G.E. Meijer

Department of Biomedical Signals and Systems,
Faculty of Electrical Engineering,
Mathematics and Computer Science,
University of Twente

UNIVERSITY OF TWENTE.

Contents

List of Acronyms

DBS Deep brain stimulation

LFP Local field potential

PD Parkinson's disease

PLV Phase locking value

SL Stuart Landau

tACS Transcranial Alternating Current Stimulation

Abstract

Introduction Deep brain stimulation (DBS) is effective in treating the motor symptoms of Parkinson's disease (PD), however, its therapeutic mechanism is still under discussion. We hypothesized that weak electric fields desynchronize cortical neurons in the motor cortex, thereby contributing to the therapeutic mechanism of DBS. For low-frequency brain stimulation (i.e. TACS), experimental and computational studies showed desynchronization by low-amplitude electric fields. In this study, we used computational models to investigate under which conditions neurons synchronize and desynchronize when an alternating weak electric field is applied.

Methods We simulated a simple oscillator model (Stuart-Landau model) to predict the behaviour and synchrony of a neural population. The effect of an external drive on the amplitude of this oscillator was investigated. To study the effect on single cells we used morphologically realistic neural models and simple two-compartment models with a synaptic input and an applied external electric field. The effect of stimulation settings on the entrainment to this applied electric field and synaptic input was studied.

Results The Stuart-Landau model showed that desynchronization can occur at high stimulation frequencies, similar to those used in DBS. For specific parameter settings, weak fields decreased entrainment, and strong fields increased entrainment. However, the relationship between stimulation amplitude and (de)synchronization is very sensitive to variations in stimulation frequency, intrinsic frequency and their ratio. The two single-cell models showed synchronization with respect to the stimulation frequency. They also showed constant synchrony with respect to the β frequency, except for the two-compartment model with a constant input, where a desynchronization to the β frequency was found. However, this was likely due to a very unrealistic neuron model that is very susceptible to noise.

Conclusion The hypothesis cannot be rejected or accepted using these models. The single-cell models in their current form are insufficient to model the baseline state (oscillatory synchrony that is not due to external inputs). However, including network interactions in this model enables future research to more accurately investigate (de)synchronization dynamics.

Chapter 1

Introduction

Parkinson's disease (PD) is a complex neurological disorder. The most prominent symptoms are the classical Parkinsonian motor symptoms such as akinesia, bradykinesia, rigidity and resting tremor [1, 2]. These symptoms arise from the degeneration of dopaminergic neurons in the basal ganglia, leading to a deficiency in dopamine [1, 3–6].

This dopamine deficiency results in excessive synchronized oscillatory activity in the basal ganglia [4, 7]. A review study by Hammond et al. [8] summarized studies that recorded local field potentials (LFP) in PD patients. Recordings from ten different studies showed oscillations in the frequency range of (8-30 Hz) in PD patients without treatment. It has been proposed that these beta oscillations indicate increased synchronization in the whole basal ganglia loop [2, 8, 9]. These beta-band oscillations have been linked to rigidity and bradykinesia [9, 10]. Hammond et al. [8] also reviewed animal studies, which support the important role of the oscillations between 8-30 Hz in the pathophysiology of motor symptoms. This increase in synchronization is also present in the primary motor cortex, which plays an important role in the pathology of PD motor symptoms [11–13].

The initial focus of PD treatment lies on replacing this dopamine depletion [14]. However, over time, the therapeutic effects can become unpredictable in the outcome and side effects [15]. For these patients, deep brain stimulation (DBS) [2, 8, 14] may be considered. Electrodes for DBS are surgically implanted in the basal ganglia to deliver current pulses, with amplitudes typically ranging from 0.7 to 4 mA [16]. DBS is an effective technique to treat motor symptoms in PD patients [2, 17–20]. However, some patients experience severe side effects [21, 22] or insufficient relief of symptoms after DBS treatment [19, 20]. To improve DBS, knowing the therapeutic mechanisms of the stimulation is essential, yet these mechanisms are still under discussion [5, 20, 23].

With DBS, frequencies above 100 Hz are used to reduce motor symptoms. However, the mechanism behind this is unclear [17, 19]. It is known that DBS affects not only the tissue at the electrodes but also its afferent and efferent targets [24], this way DBS affects the whole basal ganglia-thalamocortical loop [23]. The therapeutic mechanism of DBS may be explained by several distinct processes. Briefly stated, three main sorts of mechanisms [25] have been put forth: inhibition of the basal ganglia output, antidromic activation of the motor cortex and disruption of the firing dynamics in the basal ganglia. It also has been proposed that desynchronization of motor cortex neurons holds therapeutic significance [24, 26].

We hypothesize that the electric field from DBS does not solely affect the neurons at the direct stimulation site (subcortical neurons in the target region), but also neurons further away (cortical neurons). Hypothetically, the subcortical neurons experience a strong electric field and are synchro-

nized by this field, while the cortical neurons are exposed to a weaker field and are desynchronized by this. We hypothesize that these two effects combined result in the desynchronization of the basal ganglia-thalamo-cortical loop and restore motor control.

Weak electric fields are hypothesised to desynchronize neurons, based on studies of transcranial alternating current stimulation (tACS) [27–29]. The authors of these papers found that the synchrony was dependent on the initial synchrony and the amplitude of the electric field. Low field strength leads to desynchronization, whereas higher field strength leads to synchronization. Krause et al. [27] were the first to find a decrease in synchrony in in-vivo experiments. They explained this effect with a phenomenological oscillator model, which represents the synchrony within a neural population.

In-silico single-cell models [29] revealed a small, but consistent desynchronization at low amplitudes and synchronization at higher amplitudes. Similarly, network models [28] showed this same relationship, but with more pronounced differences in synchrony. Because single-cell models lack interactions with other neurons, synchrony was assessed by entrainment to specific frequencies. Tran et al. [29] defined entrainment with respect to the stimulation frequency, but initial entrainment was weak, limiting the potential for desynchronization. Thus, computational neuron models have already been used to study the effect of weak electric fields on synchrony [27–29] and serve as a valuable tool for predicting neuronal dynamics. These models allow for the exploration of a wide parameter space in a shorter time frame compared to experimental studies.

We will investigate under which conditions neurons synchronize and desynchronize after applying a weak electric field using computational models. Especially the influence of the stimulation amplitude will be of importance, to see if the same pattern of (de)synchronization that was found in other studies [27–29] can be found for higher frequencies and the waveform as used with DBS. Moreover, the initial synchrony will be increased to investigate whether that increases the desynchronization effect. This leads to the following research question: "Under which conditions do neurons synchronize and desynchronize when an alternating weak electric field is applied?". The synchrony with respect to the pathological β-frequencies (8-30 Hz) is most important since this thesis is in the context of PD patients. We use two models that have already been used to study the effect of TACS on synchrony: a simple oscillator model [27] and a complex multi-compartment single-neuron model [29]. Additionally, a simple two-compartment single-neuron model [30] is used. This model is less computationally expensive than the multi-compartment model but has not been used to investigate the effect on synchrony.

Chapter 2

Background information

Computational models have been used to investigate the neural response to low-frequency weak electric fields. The different types of models that are used in this thesis are oscillator models and single-cell models.

2.1 Oscillator models

Krause et al. [27] performed experiments measuring single unit recordings from V4 neurons and the ongoing LFP, during tACS. They implanted electrodes in primates to perform these measurements. The study focused on calculating the entrainment of single neuron spikes relative to the LFP, which represents synchrony within the neural population. Before tACS was applied, many neurons exhibited an initial entrainment to the 5 Hz component of the ongoing oscillations. During tACS, this entrainment often decreased, especially in neurons with a higher initial entrainment. It is important to note that during tACS, the LFP was predominantly influenced by the tACS signal.

Krause et al. [27] also observed a shift in phase preference during tACS, both in neurons whose phase locking value (PLV) was affected by tACS and in those whose entrainment remained unchanged. When the current intensity was increased, they found a specific pattern where low amplitude stimulation partially reduced entrainment, while high amplitude stimulation led to an increase in entrainment. Krause et al. used the Stuart-Landau (SL) model to explain their experimental results. They simulated an oscillator with an external drive (Figure 2.1). The dynamics of this model exhibit oscillations. It is assumed that the amplitude of these oscillations represents the synchrony within a neural population. A small mismatch between the frequency of the oscillations of the oscillator and the stimulation frequency resulted in a decrease in synchrony. While increasing the amplitude led to an increase in synchrony. Experimentally, neurons that showed a decrease in synchrony also had a frequency preference slightly lower than the 5 Hz tACS stimulation.

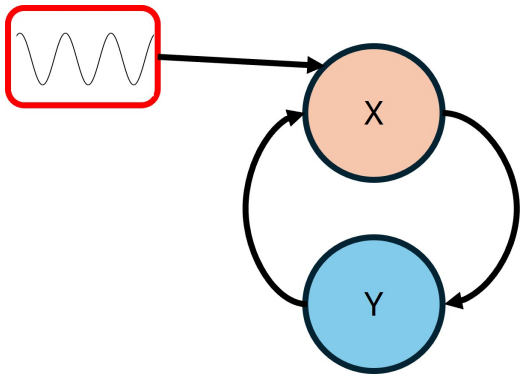

FIGURE 2.1: Schematic representation of the SL model from Krause et al. [27]. x and y describe the dynamics of an oscillator, which are stimulated by an external electric field depicted in the red box.

Using oscillator models to understand neural oscillations is a start in understanding

(de)synchronization. However, these models are very phenomenological and often without physiological units, which makes it difficult to relate to the clinical situation. Nevertheless, they are quick and give a first insight into the effects of stimulation on neurons.

2.2 Single cell models

Two different types of single-cell models are used in this thesis: a multi-compartment model [29] and a two-compartment model [30] (Figure 2.2). The multi-compartment model is morphologically realistic, however, it requires a lot of time and computational power. Two-compartment models are quicker to compute and have the minimal spatial detail required to account for an extracellular electric field biophysically [31].

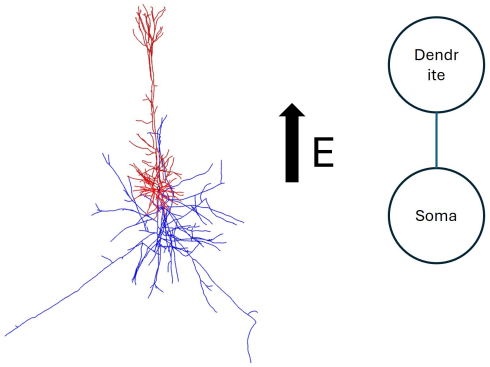

FIGURE 2.2: Schematic representation of the two single-cell models used. Where the left side represents the multi-compartment model from Tran et al. [29] and the right side the two-compartment model of Wei et al. [30]. E represents the applied electric field.

Tran et al. [29] used biologically realistic single-neuron models in the simulation environment NEURON [32] to investigate the effects of tACS. These models are multi-compartmental conductance-based and include the detailed dendritic morphology, which plays a key role in the dynamic behaviour of a neuron [33]. They observed an increase in entrainment for layer 5 pyramidal cells when increasing the electric field strength. Entrainment was quantified using the PLV relative to the stimulation waveform and used as a measure of synchrony. Their results showed a slight decrease in PLV for field intensities between 0 and 0.7 V/m, which, though small, was consistent across different layer 5 pyramidal cells. Importantly, the initial PLV without stimulation was already low, leaving limited room for further decrease.

The models that Tran et al. [29] used originate from the Blue Brain project. In the Blue Brain project, Markram et al. [34] and Ramaswamy et al. [35] made digital reconstructions of the morphology of juvenile rat cortical neurons. These reconstructions discretize the cell morphology into small compartments of length dx. The cable equation is numerically solved to calculate each compartment's membrane potential V:

$$\frac{1}{r_i}\frac{\partial^2 V(x,t))}{\partial x^2} - c_m\frac{\partial V(x,t)}{\partial t} + i_{ionic} = \frac{1}{r_i}\frac{E_{||(x,t)}}{\partial x}, \tag{2.1}$$

where c_m is the membrane capacitance, r_i is the membrane resistance (per unit length) and t is time. $E_{||}$ is the electric field induced along the neuron branch and i_{ionic} represents the ionic currents. Markram et al. [34] added thirteen different ionic channels to the different components of the neuron model. To calculate the ion channel conductances, they employed a multi-objective optimization technique [36]. The conductances were selected so that the model's behaviour aligns with experimental electrophysical data, such as the amplitude, spike width, and spike rate.

Aberra et al. [37] and Tran et al. [29] used the models from the Blue Brain project [34, 35] to investigate the effects of brain stimulation. Aberra et al. [37] first adapted the neuron models by

adding myelination to the axons and translated them to human brain cells. They did this by changing geometric parameters, such as the length and diameter of dendrites and other cell components. Second, they implemented intracortical microstimulation and direct current electric fields. Tran et al. [29] continued with the human neuron models from Aberra et al. [37] and added a synaptic input to these models. They did this to ensure activity without stimulation, and to investigate subthreshold stimulation effects.

Tran et al. [29] added a synapse to manifest a baseline spike rate of 5 Hz. They modelled the synaptic activity with a two-exponential function:

$$I_{syn}(t) = g_{syn}(t)(V(t) - E_{syn}), \tag{2.2}$$

$$g_{syn}(t) = w\frac{\tau_1\tau_2}{\tau_1 - \tau_2}\left(\exp(-\frac{t}{\tau_1}) - \exp(-\frac{t}{\tau_2})\right), \tag{2.3}$$

where $E_{syn} = 0$ mV is the synaptic reversal potential, g_{syn} the synaptic conductivity, w is the weight of the synapse, $V(t)$ is the membrane potential and $\tau_1 = 2$ ms and $\tau_2 = 10$ ms are the rise and decay time of the synapse. The synapse is activated at time t each time there is a synaptic input. The synaptic input of this synapse is a spike train of 50 Hz with a Poisson distribution. This synapse has a seed generator to ensure the same noise within different simulations. They adjusted the weight and location of the synapse to reach a baseline spike rate of 5 Hz.

The interaction between the applied electric field and the neuron is simulated as explained by Tran et al. [29], using the extracellular mechanism of NEURON. For each compartment, the extracellular potential caused by the stimulation is computed with the quasipotential. The field is spatially uniform and applied in the direction of the somatodendritic axis of the cell, therefore the quasipotential can be estimated by:

$$V^i = E * d, \tag{2.4}$$

where V^i is the extracellular potential of the i^{th} compartment, E is the electric field strength and d the distance between the compartment and the cathode.

Wei et al. [30] employed a reduced version of the Pinsky–Rinzel (PR) model, which is a two-compartment model that has been thoroughly investigated in constant electrical fields [38–40]. Wei et al. [30] investigated the effects of the amplitude and frequency of a sinusoidal electrical field on the firing pattern of neurons and how this depends on the morphology of the cell. Their findings demonstrated that morphology influences a neuron's dynamical behaviour and its dependence on the amplitude and frequency of the electrical field. This model has not been used in the context of synchrony yet.

Entrainment

In single-cell models, the consistency of the phase relationship between the spikes of neurons and a continuous signal with a constant frequency (entrainment) can be used as a synchrony measure. This consistency can be calculated using pairwise phase consistency (PPC), PLV and coherence [41]. Vinck et al. [41] showed that the PPC does not have any biases, whereas the PLV and coherence are biased for finite sample sizes. The PPC computes the vector dot product for each possible pair of relative phases. This dot product represents how similar the two relative phases are.

$$PPC = \frac{2}{N(N-1)}\sum_{j=1}^{N-1}\sum_{k=(j+1)}^{N} f(\theta_j, \theta_k), \qquad f(\phi, \omega) = \cos(\phi)\cos(\omega) + \sin(\phi)\sin(\omega) \tag{2.5}$$

The PPC ranges from -1 to 1, where -1 indicates no entrainment and 1 signifies complete entrainment. It is rescaled to the PLV using the following equation:"[41]:

$$\text{PLV} = \sqrt{\max(0, \text{PPC})}. \tag{2.6}$$

Whereas the standard method of calculating the PLV is:

$$PLV = \left| \frac{\sum_{k=1}^{N} e^{i\theta_k}}{N} \right|, \tag{2.7}$$

where N is the total number of spikes, and θ_k the phase of the kth spike. The PLV ranges from 0 to 1, where 0 indicates no entrainment and 1 total entrainment.

Chapter 3

Methods

3.1 Stuart-Landau model

The code from Krause et al. [27] was used to implement the SL model. The following equations describe the SL model:

$$\frac{dx}{dt} = \lambda x - 2\pi f y - \gamma(x^2 + y^2)x + ks(t), \tag{3.1}$$

$$\frac{dy}{dt} = \lambda y + 2\pi f x - \gamma(x^2 + y^2)y, \tag{3.2}$$

where $s(t) = \sin(2\pi f_s t)$ and x and y are the state variables that describe the dynamics of an oscillator, which is stimulated with a sinus with frequency f_s and amplitude k. The parameters λ and γ control the stability and damping of the system, respectively. Parameter f represents the frequency of the ongoing oscillations of the oscillator (intrinsic frequency). The model does not have physical units. However, we assume that the time is in s and the frequency in Hz, similar to in Doelling et al. [42]. The parameter settings were the same as in Krause et al. [27]: $\lambda = 0.2, \gamma = 1.0$ and $f = 0.5$ Hz. The amplitude k ranged between 0% and 100% of the amplitude of the signal without stimulation, calculated by taking the root-mean-squared value times $\sqrt{2}$.

The stimulation frequency varied between 0 and 150 Hz, to investigate the effects of stimulation frequencies used for DBS on (de)synchronization. The step size was 1 Hz, except for the frequency range close to the intrinsic frequency, where it was 0.01 Hz. The stepsize was smaller around the intrinsic frequency because Krause et al. [27] showed desynchronization close to the intrinsic frequency. For an intrinsic frequency of 0.5 Hz, this range was between 0 and 1 Hz, for the other intrinsic frequency this was between $f_{intrinsic} - 2$ Hz and $f_{intrinsic} + 2$ Hz.

Entrainment
Just as in Krause et al. [27], it was assumed that the amplitude of the oscillations generated by the SL model represents the synchrony of a neural population. In Matlab, the differential equations were solved using the Matlab ODE45 solver. The stimulation $s(t)$ was switched on after 40 s, so the model could first become stationary before the drive was applied. The simulations were carried out for different phase lags between the stimulus and the ongoing oscillation: $(0, \frac{\pi}{4}, \frac{\pi}{2}, \frac{3\pi}{4}, \pi, \frac{5\pi}{4}, \frac{3\pi}{2}, \frac{7\pi}{4})$, which were averaged. The initial conditions were: $[x, y] = [0, -1]$. Simulations were run for different stimulation frequencies and amplitudes. For each simulation, the difference in amplitude between the stimulated condition and the control condition was calculated. The amplitude of the simulation was defined as $\sqrt{2}$

times the root–mean–squared value of the signal. In the case of the control condition, the amplitude of the stimulation was zero, meaning there is no stimulation. If the difference is positive, there is an increase in entrainment, and if the difference is negative, there is a decrease in entrainment.

Simulations

In this thesis, we reproduced the results of Krause et al. [27]. Next, the stimulation frequency was increased to vary between 0 and 150 Hz and the intrinsic frequency was set to: 0.5, 4, 8, 12 and 16 Hz. This increase in intrinsic frequency represents the pathologial β synchrony. The ratio ($f_{stim}/f_{intrinsic}$) between these two frequencies is shown in a secondary x-axis. Since the stimulation amplitude remained constant across intrinsic frequencies, the maximal ratio decreased as the intrinsic frequency increased. To assess the impact of this ratio, we computed the ratio where the entrainment shows the biggest decrease and increase. For a fair comparison, this computation was restricted to ratios present in all settings, with a maximum value of $150/16 = 9.375$. Only ratios bigger than 2 were included.

3.2 Multi-compartment model

To simulate the behaviour of a single cell, we used the code from Tran et al. [29], implemented in the simulation environment NEURON version 8.0.1. In this thesis, only the layer 5 pyramidal cells were used, since these are the cells in the primary motor cortex, which are most susceptible to an electric field [43].

Stimulation
Two stimulation waveforms were used: a sinusoidal waveform as used in tACS [29] and a typical DBS waveform [44, 45]. This waveform is visualized in Figure 3.1 and consists of a cathodic phase, an interphase interval followed by a passive recharge phase. The duration of these phases is based on literature [44, 45]. The cathodic stimulus is a negative block pulse with the amplitude of the DBS and a duration called pulse width, which was set to 125 μs. The interphase was 75 μs and the recharge phase was 4 ms. The recharge phase has a positive amplitude which decays over time. The amplitude of this phase was chosen such that the total charge is zero.

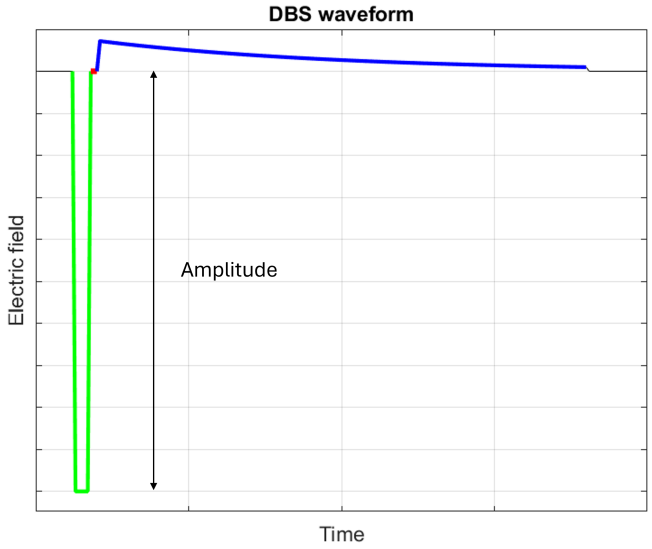

FIGURE 3.1: Typical DBS waveform with cathodic phase (green), interphase (red) and passive recharge phase (blue).

As discussed in Chapter 2, the electric field was applied along the somatodendritic axis of the cell. However, due to the cortical folding, pyramidal cells may exhibit varying orientations, leading to differences in the direction of the electric field experienced by each cell. Consequently, the DBS waveform was applied in two configurations. In the first, a negative pulse (Figure 3.1) resulted in a negative potential at the soma relative to the dendrite. In the second, a positive pulse-where the waveform was inverted- produced a positive potential at the soma relative to dendrite. This approach allowed for stimulation in both polarities, referred to as DBS-negative, corresponding to the waveform in the figure, and DBS-positive, which represents the inverted waveform.

Entrainment
When a simulation was run in NEURON, the variables over time were exported in textfiles. These text files were loaded into MATLAB R2024a for further analysis. Tran et al. [29] wrote a script which detects the times at which an action potential occurs (spike times), by monitoring when the membrane

potential in the soma exceeds a threshold of 0 mV. These spike times were also exported in a text file. With these spike times, we computed the relative phase of each spike with respect to a sinusoidal wave with a constant frequency. With these relative phases and the code from Vieira et al. [46], we calculated the PPC. This code calculates the PPC in a fast and numerically stable way. To compare with other articles, the PPC was transformed to the PLV using equation (2.6). To calculate the PLV according to the standard method, equation (2.7) was implemented in Matlab.

3.2.1 Original parameter settings

First, we ran the model with only the first synapse, with a weight of 0.015 and a distance of 334 μm to the soma. we simulated 245 s of data, where stimulation started after 5 s. The stimulation was sinusoidal with a frequency of 10 Hz and amplitudes ranging from 0 to 3 V/m, with steps of 0.1 V/m up to 2 V/m and steps of 0.2 V/m between 2 and 3 V/m. These parameter settings were the same as in Tran et al. [29] and were chosen to reproduce their results. The entrainment was calculated with respect to the stimulation frequency, using both the standard PLV method and the PPC method.

3.2.2 Adjusting stimulation waveform and frequency

Next, the influence of the different stimulation waveforms (sinusoidal, DBS-positive and DBS-negative) and stimulation frequencies (10 and 130 Hz) was investigated. This was done with an without baseline activity (with and without synapse).

One synapse
The same synaptic configuration as described above was used to investigate the effect of different waveforms and stimulation frequency on the entrainment with respect to the simulation frequency and the spikerate. The simulations generated 125 s of data using the stimulation amplitudes as described above, with stimulation starting after 5 s. The three different waveforms were tested with both 10 Hz and 130 Hz. The entrainment was calculated with respect to the stimulation frequency using the PPC method.

No synapse
To further research the differences between the two waveforms and to characterize the dynamic behaviour of the model, the synapses were removed (so there is no baseline activity). For different stimulation frequencies (10 to 150 Hz with steps of 20 Hz) and amplitudes (0 to 170 with steps of 10 V/m), the spike rate after stimulation is computed. This was done on 10 s of data.

3.2.3 Addition of synapse with beta input

We increased the weight of the first synapse to get a baseline spike rate between 8.5 and 9.5 Hz because the motor cortex's ongoing spontaneous activity was characterized by individual neurons irregularly firing at a low average spike rate (<10 Hz), but a broad frequency range (0-100 Hz) [47]. The weight of the synapse was increased to 0.016 and the distance of the synapse was changed from 334 μm to 117 μm.

Furthermore, a new synapse with presynaptic input of 11 Hz was added, to ensure a high initial entrainment. This was done to investigate if increasing the initial entrainment, enhances the desynchronization effect observed by Tran et al. [29] during 10 Hz sinusoidal stimulation. Therefore 10 Hz sinusoidal stimulation was used. The 11 Hz signal represented the pathologically synchronized beta activity present in PD patients. The choice for this frequency is also supported by Krause et al. [27] who found a desynchronization effect when the stimulation frequency was close to the intrinsic frequency.

The presynaptic input was either deterministic or jittered. For deterministic input, the intervals between spikes were fixed at 1/11 s. In the jittered condition, the intervals between spikes were not fixed but varied around this base period to represent a more realistic synaptic input. This variation was achieved by adding a random jitter value, which is uniformly distributed between $-\frac{\text{jitter percentage}}{2}\%$ and $+\frac{\text{jitter percentage}}{2}\%$ of the base period, to each spike interval. The jitter percentages used are: 5%, 10% and 20%. The weight of both synapses was changed so that the initial entrainment was higher than without the extra synapse and the spike rate stayed between 8.5 and 9.5 Hz.

The second synapse was added to the same location as the first, with its weight set to either 0.005 or 0.009 and jitter varied at 0%, 5%, 10%, or 20%. The neuron was stimulated with a sinusoidal waveform of 10 Hz. We simulated 125 s of data, where stimulation started after 5 s. This was done for a wide range of amplitudes between 0 and 10 V/m, with a step size of 0.1 V/m between up to 1 V/m, 0.2 V/m between 1.0 and 3.0 V/m, 0.5 V/m between 3.0 and 5.0 V/m and 1.0 V/m between 5.0 and 10.0 V/m. The entrainment was calculated using the PPC method to both the stimulation frequency (10 Hz) and the intrinsic pathological frequency (11 Hz).

Generating 120 s of data on my laptop (Intel Core i5-8265U CPU 1.6 GHz, 4 cores, 8 threads) took 1500 minutes. On the EEMCS-HPC cluster of the University of Twente, 30 simulations were run in parallel in one job, using 2 CPUs per task. Multiple jobs could be submitted at the same time, depending on the availability of the server, with a maximum of 8 jobs.

3.3 Two-compartment model

The model of Wei et al. [30] that was used is visualised in Figure 3.2. We implemented this model in a Capita Selecta to investigate the effect of the morphology on the spike rate during stimulation. There were two compartments in the model: the soma and the dendrite. The somatic compartment had two active ionic currents (I_{Na} and I_K), a capacitive current and a passive leakage current (I_{SL}). The dendritic compartment included only capacitive and passive leakage currents (I_{DL}). Parallel to the somatic-dendritic axis, an extracellular electric field was applied (V_{AC}).

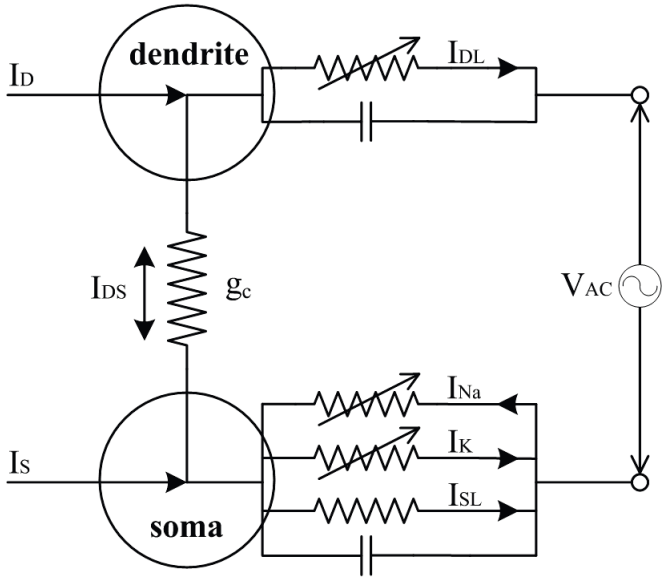

FIGURE 3.2: Schematic representation of the two-compartment model. Figure adapted from: [30].

The model is described by the following equations:

$$C_m \frac{dV_S}{dt} = \frac{I_S}{p} + \frac{I_{DS}}{p} - \bar{g}_{Na} m_\infty(V_S)(V_S - E_{Na}) - \bar{g}_K w(V_S - E_K) - g_{SL}(V_S - E_{SL}), \tag{3.3}$$

$$C_m \frac{dV_D}{dt} = \frac{I_D}{(1-p)} - \frac{I_{DS}}{(1-p)} - g_{DL}(V_D - E_{DL}), \tag{3.4}$$

$$\frac{dw}{dt} = \varphi_w \frac{w_\infty(V_S) - w}{\tau_w(V_S)}, \tag{3.5}$$

$$V_{AC} = A \sin(2\pi f t), \tag{3.6}$$

$$I_{DS} = g_c(V_{AC} + V_D - V_S), \tag{3.7}$$

$$m_\infty(V_S) = 0.5 \left(1 + \tanh\left(\frac{V_S - \beta_m}{\gamma_m}\right)\right), \tag{3.8}$$

$$w_\infty(V_S) = 0.5 \left(1 + \tanh\left(\frac{V_S - \beta_w}{\gamma_w}\right)\right), \tag{3.9}$$

$$\tau_w(V_S) = \frac{1}{2} \cosh\left(\frac{V_S - \theta_w}{2\sigma_w}\right). \tag{3.10}$$

where V_S and V_D correspond to the membrane potentials in the somatic and dendritic compartments and w is the activation variable for the potassium channels. V_{AC} is the applied electric field, where f is the frequency and A the amplitude of the field. The morphological parameter p is the proportion of area occupied by the soma. I_S and I_D are the synaptic inputs. The current between the soma

and dendrite is denoted by I_{DS} and the connectivity between the two compartments is represented by g_c. Equations (3.8), (3.9), and (3.10) are the voltage-sensitive steady-state activation functions and the time variable. Table 3.1 summarizes the parameter values, the initial conditions are set as $[V_S, V_D, w] = [-70mV, -70mV, 0]$.

TABLE 3.1: Parameter values [30].

Parameter	Value	Parameter	Value
E_{Na}	50 mV	C_m	2 $\mu F/cm^2$
E_K	-100 mV	β_m	-1.2 mV
E_{SL}	-70 mV	β_w	0 mV
E_{DL}	-70 mV	γ_m	18 mV
g_{Na}	20 mS/cm^2	γ_w	10 mV
g_K	20 mS/cm^2	ϕ_w	0.15 (unitless)
g_{SL}	2 mS/cm^2	g_c	1.0 mS/cm^2
g_{DL}	2 mS/cm^2	I_s	0 mA

Noise was added to the membrane potential of the dendrite to simulate a more realistic scenario, where there are small fluctuations in resting membrane potential and evoke some baseline activity. This noise was added using the Euler-Maryuana scheme:

$$\mathbf{x}_{k+1} = \mathbf{x}_k + f(t_k, \mathbf{x}_k)dt + \sigma\sqrt{dt}\mathbf{g}\xi_k, \tag{3.11}$$

where: $\mathbf{x}_k$ is the state vector at the k-th time step, dt is the time step size, $f(t_k, \mathbf{x}_k)$ is the deterministic part of the update, represented by the equations (3.3), (3.4) and (3.5). σ is the standard deviation of the noise. $\mathbf{g}$ is a vector that specifies how the noise is applied to different components of the state vector, in this case $\mathbf{g} = \begin{bmatrix}0 & 1 & 0\end{bmatrix}$, meaning the noise only affected the second component. $\xi_k \sim \mathcal{N}(0, 1)$ is a standard normal random variable, generated by 'randn()' in MATLAB.

Stimulation
Stimulation was a sinusoidal waveform and its amplitude was expressed in mV. In the multi-compartment model, the amplitude was expressed in V/m. The length of the apical dendrite of a layer 5 pyramidal cell varies a lot and can reach lengths of up to 2 mm [48]. The multi-compartment model had an apical dendrite of approximately 1000 μm, meaning that an amplitude of 1 mV results in an electric field of 1 V/m.

Entrainment
The spikes were calculated using the findpeaks function in MATLAB with a threshold of 0 mV. Next, the PPC method explained in section 3.2 was used to calculate the entrainment to the intrinsic frequency and stimulation frequency.

3.3.1 Constant synaptic input

The synaptic input was only applied at the dendrite, the synaptic input to the soma (I_s) is zero. This was done to ensure a baseline spike rate and entrainment without stimulation. Since the synaptic input was constant, the intrinsic frequency was defined differently from the multi-compartment model. The spike rate without stimulation was considered the intrinsic frequency since this was the frequency the neuron was entrained to without stimulation. The synaptic input was set to a constant value of 77 $\mu A/cm^2$. Simulations were performed for to values of σ: $\sigma = 0$ and $\sigma = 0.0125$. The stimulation amplitude varied from 0 mV and 1 mV in increments of 0.05 mV. The frequency was changed from 10 to 150 Hz with increments of 20 Hz. The entrainment was calculated using the PPC method on

two different frequencies: the stimulation frequency and the baseline spike rate of the neuron without stimulation. Simulations of 120 s were generated for one seed.

3.3.2 Exponential synaptic input

Next, the synaptic input was changed to a more realistic synapse using equations (2.2) and (2.3). The synaptic reversal potential and rise and decay time were the same as for the multi-compartment model. Similar to the multi-compartment model, two synaptic inputs were incorporated: one Poisson-distributed synapse with a firing rate of 50 Hz, and a second synapse with a regular firing rate of 11 Hz. Weights were chosen such that there is an initial PLV around 0.1-0.2 to 11 Hz and the spike rate was between 10 and 11 Hz. Seven different synaptic configurations were simulated, where the weights of both synapses vary. To obtain a more realistic scenario, the noise level σ was increased to 10. The entrainment was calculated with respect to the stimulation frequency (10 Hz) and the frequency of the regular synapse (11 Hz). This was done using the PPC method on 120 s of data from six different seeds.

Chapter 4

Results

4.1 Stuart-Landau model

Figure 4.1 shows an example of a time series of the SL model. As explained in chapter 3.1, the entrainment was computed by taking the difference between the amplitudes of the oscillations with and without stimulation, here represented by the dashed lines.

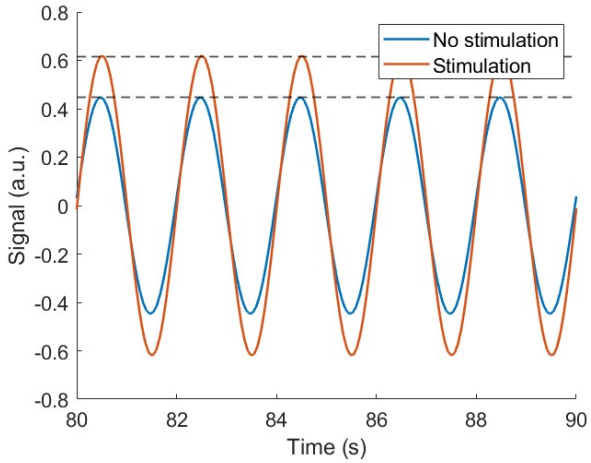

FIGURE 4.1: Example of a time series of a simulation of the SL model. The dashed line respresents the amplitude defined by the root-mean-squared value of the signal multiplied by $\sqrt{2}$. The amplitude of the stimulation is 50% of the baseline amplitude.

4.1.1 Replication of Krause et al.

The change in entrainment across a range of stimulation frequencies and stimulation amplitudes is shown in Figure 4.2. For a stimulation frequency close to the intrinsic frequency (Figure 4.2b), a pattern emerged where small amplitudes decrease entrainment, while high amplitudes led to an increase, replicating findings by Krause et al [27]. At higher stimulation frequencies typical of DBS, only a decrease in entrainment was observed, with no clear pattern between stimulation amplitude and change in entrainment. Additionally, the differences in entrainment between different stimulation amplitudes were minimal.

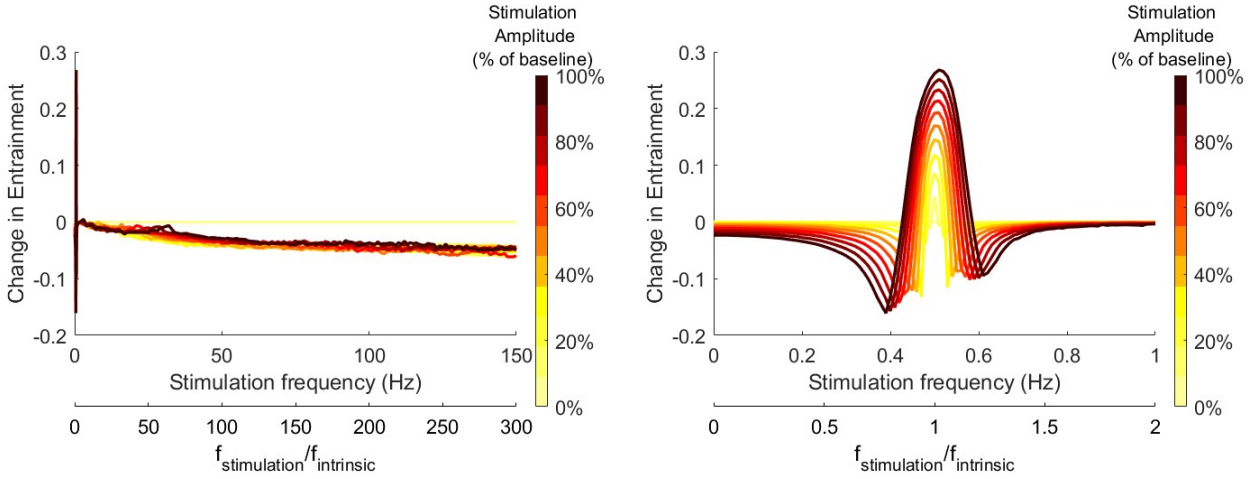

(A) Total view

(B) Stimulation frequency close to intrinsic frequency

FIGURE 4.2: Changes in entrainment dependent on stimulation frequency and amplitude for an intrinsic frequency of 0.5 Hz. The stimulation-to-intrinsic frequency ratio is visualized in a secondary x-axis. (A) shows the total range of inspected stimulation frequencies where (B) zooms in on the stimulation frequencies close to the intrinsic frequency.

4.1.2 (De)synchronization depends on the ratio of intrinsic and stimulation frequency

Increasing the intrinsic frequency of the ongoing oscillations altered the (de)synchronization pattern (Figure 4.3). For $f_{int} = 8$ Hz and $f_{stim} = 120$ Hz low fields desynchronized and high fields synchronized. In the appendix (Figure A.1), two time-series of this phenomenon are shown. In certain stimulation frequency ranges, low amplitudes yielded maximal desynchronization, whereas in others, high amplitudes yielded maximal desynchronization. Additionally, some frequency ranges showed no linear relationship between amplitude and maximal desynchronization. These patterns shifted rapidly with changes in the stimulation frequency and intrinsic frequency. This indicates that the (de)synchronization response is influenced by both the intrinsic and stimulation frequency.

To investigate the impact of the stimulation-to-intrinsic frequency ratio on the (de)synchronization pattern, the maximum changes in entrainment (both positive and negative) were detected and their corresponding amplitudes and ratios are visualized in Figure 4.4. At higher intrinsic frequencies, both maximal synchronization and desynchronization consistently occured at the same ratio. However, there are a few exceptions for desynchronization, most of which corresponded with low magnitudes of change. These results suggest that (de)synchronization patterns depend not only on the intrinsic and stimulation frequency but also on their ratio.

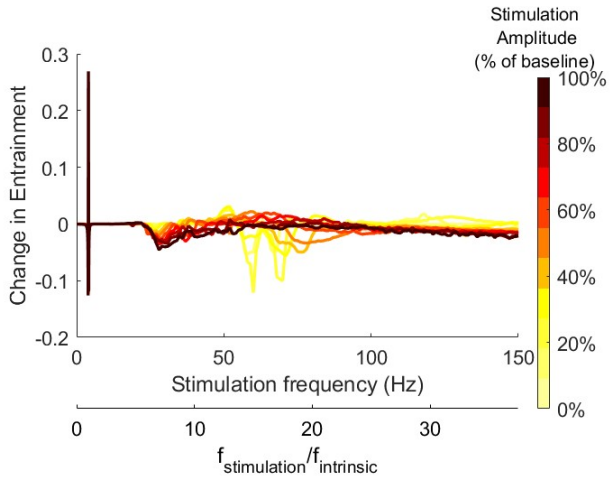

(A) Intrinsic frequency = 4 Hz

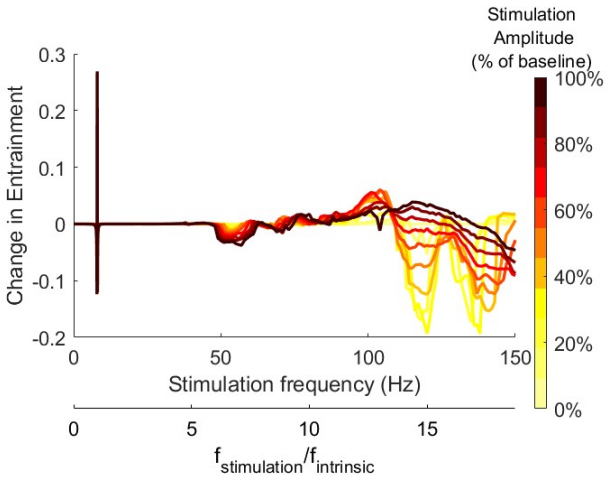

(B) Intrinsic frequency = 8 Hz

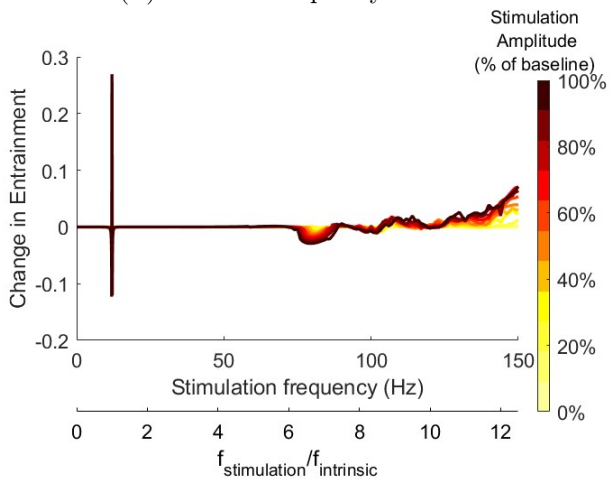

(C) Intrinsic frequency = 12 Hz

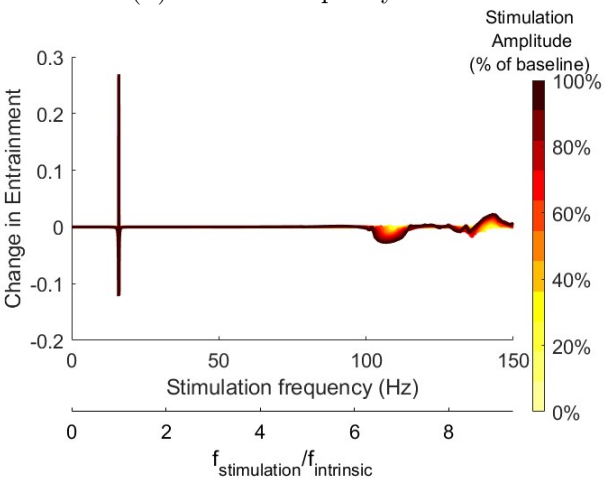

(D) Intrinsic frequency = 16 Hz

FIGURE 4.3: Changes in entrainment dependent on stimulation frequency and amplitude for different intrinsic frequencies. The stimulation-to-intrinsic frequency ratio is visualized in a secondary x-axis The secondary x-axis indicates the stimulation-to-intrinsic frequency ratio. The secondary x-axis indicates the stimulation-to-intrinsic frequency ratio.

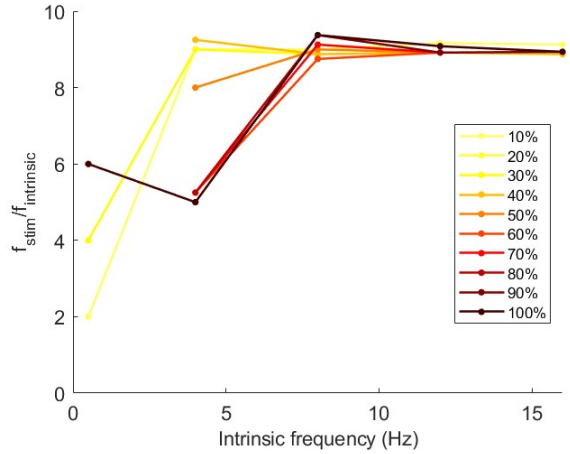

(A) Ratio ($f_{stimulation}/f_{intrinsic}$) where maximal increase in entrainment occurs

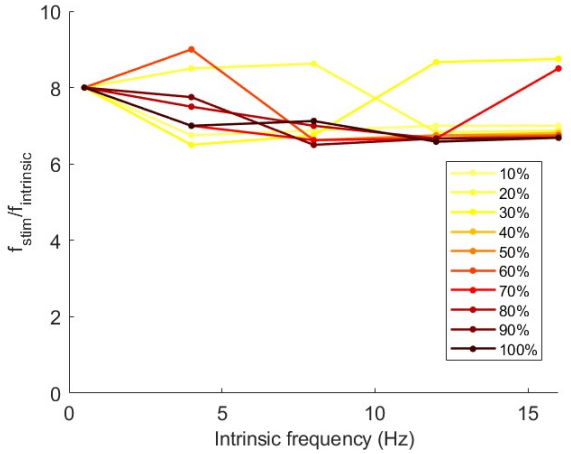

(B) Ratio ($f_{stimulation}/f_{intrinsic}$) where maximal decrease in entrainment occurs

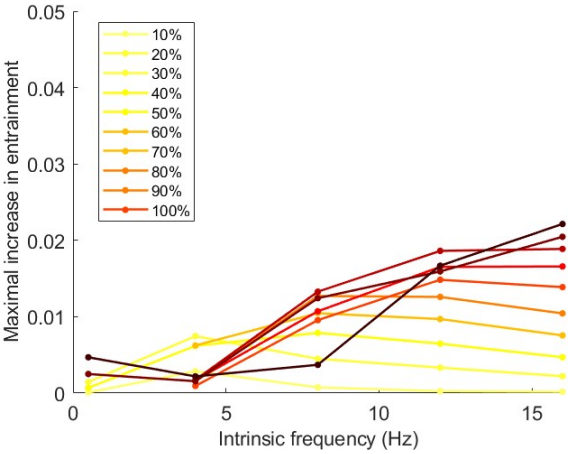

(C) Amplitude of maximal increase in entrainment

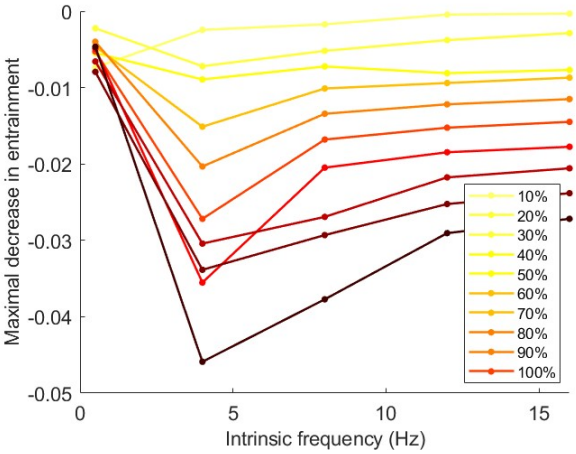

(D) Amplitude of maximal decrease in entrainment

FIGURE 4.4: Maximal change in entrainment dependant on the intrinsic frequency and the stimulation amplitude, where (A) and (B) respectively show the ratio ($f_{stimulation}/f_{intrinsic}$) and the magnitude of the maximal increase, whereas (C) and (D) show that for the maximal decrease. Some data points are missing, due to the absence of increase/decrease.

4.2 Multi-compartment model

Figure 4.5 shows an example time series for the multi-compartment model. As explained, the spiketimes were extracted and used for further analysis.

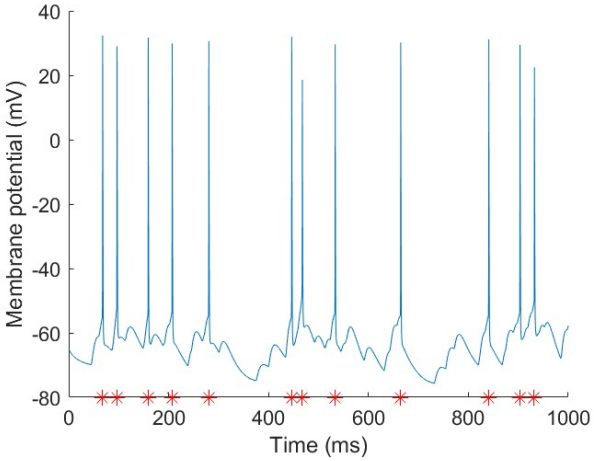

FIGURE 4.5: Example of a time series of the multi-compartment model. The stars indicate the spike times.

4.2.1 Partial replication of Tran et al.

Using the parameters from Tran et al. [29] (without an additional synapse), the PLV was calculated using both the standard method and the PPC method (Figure 4.6). The simulations were run twice with different seeds for the synaptic input of the first synapse. The desynchronization that Tran et al. [29] showed in their figure was not visible using the PPC calculation. However, when using the standard PLV method, a small desynchronization effect was observed. The magnitude of this effect varied depending on the seed of the noisy input of the first synapse. The spike rate increased with 1-2 % (appendix B Figure B.1).

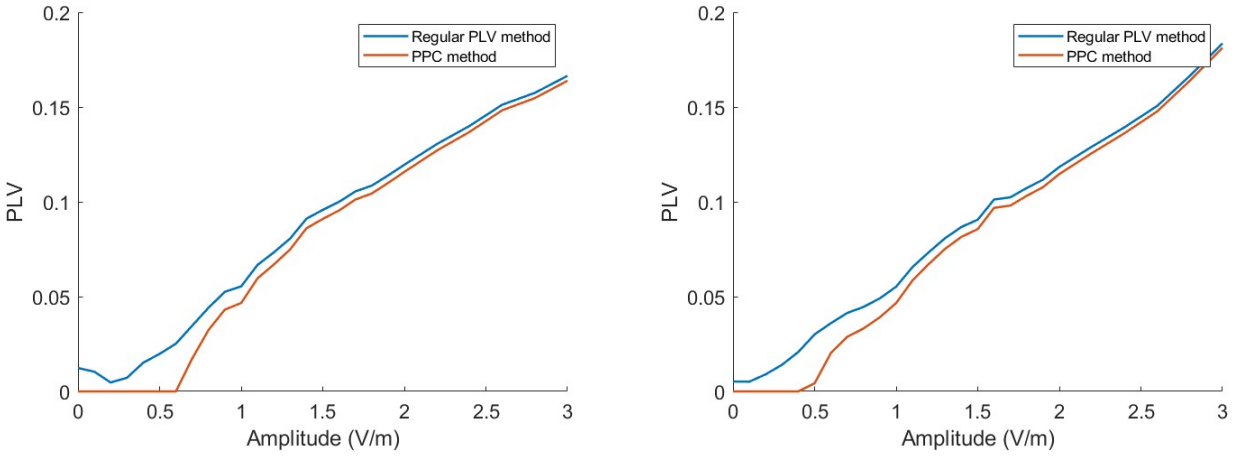

(A) seed 1

(B) seed 2

FIGURE 4.6: Entrainment to the stimulation frequency (10 Hz) as a function of stimulation amplitude for the multi-compartment model with one synapse ($w_1 = 0.015$). Stimulated with a sinusoidal waveform of 10 Hz. Calculated using the regular PLV method and the PPC method. Based on simulations of 240 s, visualised for (A) seed=1 and (B) seed=2.

4.2.2 Stimulation waveform and frequency influence entrainment and spiking threshold

Investigating the effect of different stimulation settings involved conducting simulations with the same synapse settings as before, using stimulation frequencies of 10 Hz and 130 Hz with both DBS waveforms and the sinusoidal waveform. The effect of these settings on the entrainment with respect to the stimulation frequency is visualized. Figure 4.7 shows that the sine wave of 130 Hz resulted in the fastest and highest entrainment. In contrast, neither DBS-positive nor DBS-negative waveforms produced any entrainment at stimulation amplitudes between 0 and 10 V/m.

The stimulation amplitude was incrementally increased until an increase in PLV was observed, to asses when the DBS waveforms led to an increase in entrainment (with respect to the stimulation frequency). For 10 Hz stimulation, this occurred between 50 and 60 V/m for the DBS-negative waveform and between 30 and 40 V/m for the DBS-positive waveform. For 130 Hz, no increase was observed with the DBS-negative waveform up to 230 V/m, while for the DBS-positive waveform, an increase in PLV was noted between 30 and 40 V/m. These results demonstrate that waveform type influences the entrainment threshold across different conditions.

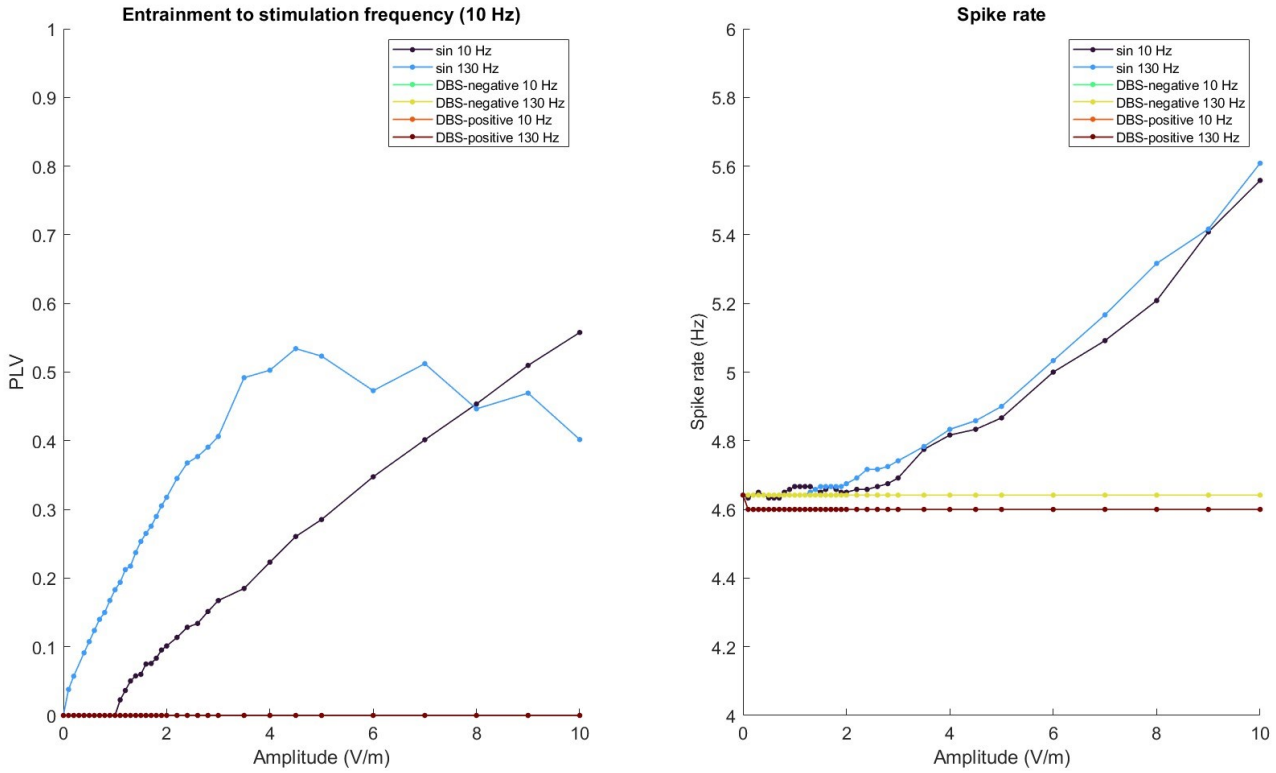

FIGURE 4.7: Entrainment and spike rate as a function of stimulation amplitude for the multi-compartment model with one synapse ($w_1 = 0.015$). Entrainment is calculated using the PPC method with respect to the stimulation frequency. Evaluated for different waveforms and stimulation frequencies. Based on simulations of 120 s of constant seed. DBS-negative 10 Hz and DBS-positive 10 Hz are not visible, because they show the exact same trend as the DBS-negative 130 Hz and DBS-positive 130 Hz, respectively.

To investigate the intrinsic properties of the model and the effects of different stimulation waveforms on the spiking threshold, simulations were conducted without synapses. In the absence of synapses, neurons exhibit no baseline spiking and only begin to spike when the stimulation amplitude exceeds a certain threshold. Figure 4.8 displays the spike rate as a function of stimulation amplitude and frequency for the three waveforms. The results indicate that DBS waveforms require higher amplitudes to induce spiking compared to the sinusoidal waveform. Additionally, the DBS-positive waveform induces spiking at lower amplitudes than the DBS-negative waveform. Moreover, it becomes clear that the model can reach spike rates up to 150 Hz when stimulated with the DBS-positive waveform.

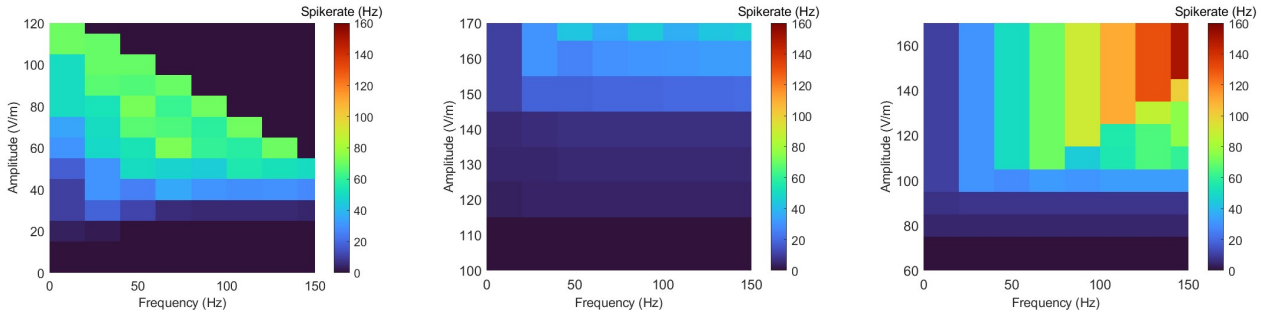

(A) Sinusoidal waveform (B) DBS-negative waveform (C) DBS-positive waveform

FIGURE 4.8: Entrainment and spike rate as a function of the stimulation frequency and amplitude, for the multi-compartment model without synapse. Evaluated for three different waveforms. Based on simulations of 10 s.

4.2.3 Increasing entrainment to β input does not enhance desynchronization

The second synapse was added to achieve an initial PLV bigger than 0 to the regular input of 11 Hz. This initial synchrony was modelled to represent pathological synchrony close to the stimulation frequency of 10 Hz. The location and weight of the first synapse were adjusted to induce a higher initial spike rate. The simulations were conducted with a sinusoidal stimulation at 10 Hz with varying parameters for the second synapse (weight and jitter percentage), and each configuration was tested with two different seeds. Figure 4.9 shows that the entrainment to the intrinsic frequency (11 Hz) did not exhibit a consistent pattern of decrease or increase. The entrainment to the stimulation frequency was initially zero in all cases and increased with the stimulation amplitude. The spike rate shows low fluctuations.

The effect of slightly higher amplitudes (between 3 and 10 V/m) was also evaluated (see Figure B.2 in appendix B), but the trend remained unchanged, except for the spike rate, which started increasing from 3 V/m.

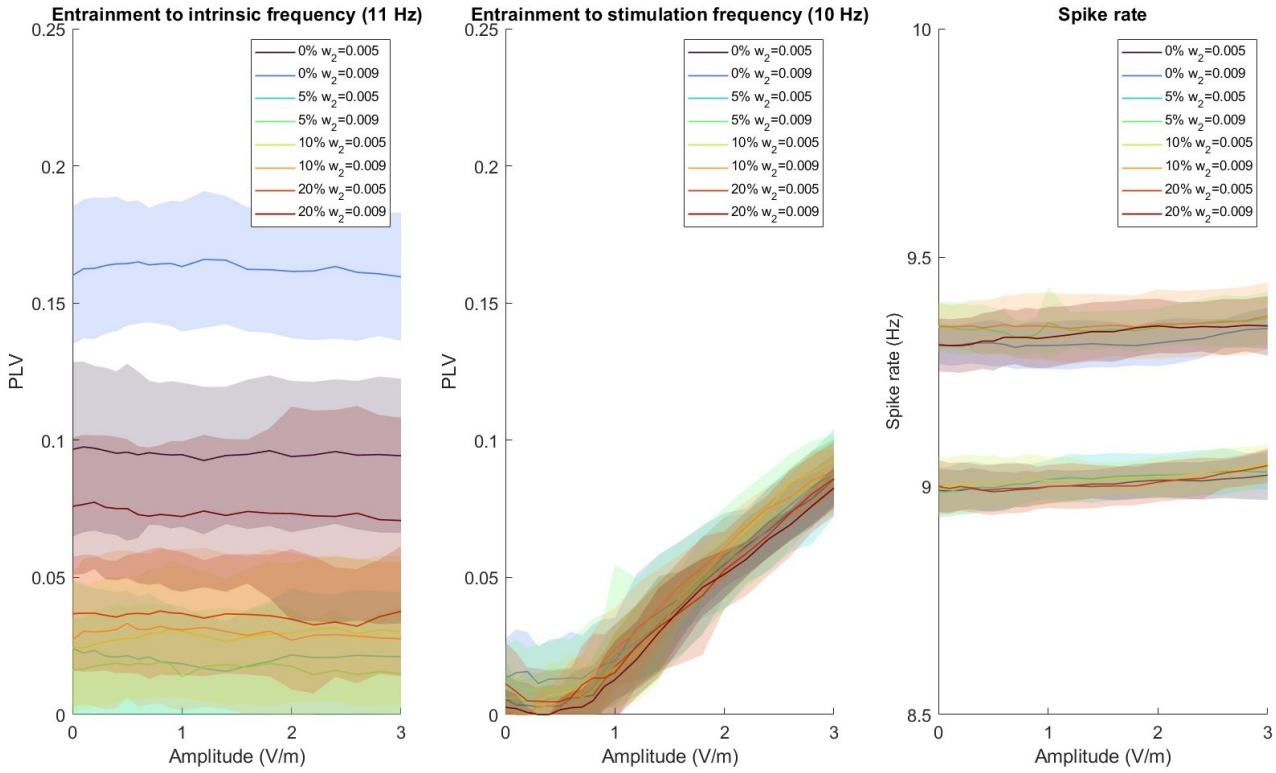

FIGURE 4.9: Entrainment and spike rate as a function of stimulation amplitude for the multi-compartment model with two synapses ($w_1 = 0.016$). The weight and jitter percentage of the second synapse is varied. Stimulated with a sinusoidal waveform of 10 Hz. Based on simulations of 120 s of six seeds. The line indicates the mean value across the seeds and the shade visualizes the standard deviation.

4.3 Two-compartment model

Two-compartment model example time series is shown in Figure 4.10 for both types of inputs.

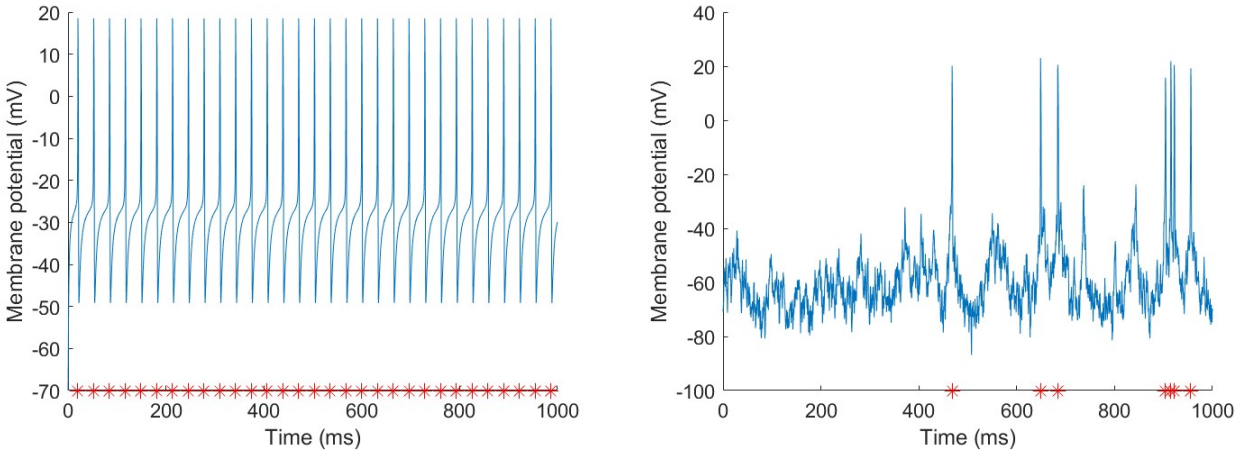

(A) Constant synaptic input

(B) Exponential synaptic input

FIGURE 4.10: Example of a time series of the two-compartment model with (A) constant input and (B) exponential synaptic input. The red stars indicate the spike times.

4.3.1 Constant input results in spiking behaviour that is easily disturbed

The two-compartment model was implemented using a constant dendritic input, designed to achieve an initial entrainment to any frequency. The constant dendritic input resulted in a very regular spiking behaviour at a specific frequency (Figure 4.10a), which was considered the intrinsic frequency for calculating the PLV. When $I_d = 77\mu A/cm^2$ and $\sigma = 0$ the baseline spike rate was 31.05 Hz. The PLV was calculated with respect to this baseline spike rate and the stimulation frequency.

4.11 illustrates that entrainment to the intrinsic frequency decreased immediately upon stimulation, while entrainment to the stimulation frequency increased. The entrainment behaviour to the stimulation frequency varied with the stimulation frequency. All the stimulation frequencies that were tested, are visualized in the appendix (Figure C.1 in the appendix). When the stimulation frequency was lower than the baseline spike rate ($f_{stim} = 10$ Hz, baseline spike rate=30 Hz), there was a sudden decrease in PLV and bursts occured (Figure C.2 in the appendix). Initially, the burst consisted of two spikes per cycle, but as the stimulation amplitude increased, bursts with three spikes per cycle occured. These bursts aligned with the 10 Hz stimulation frequency, but each burst contained three spikes, matching the baseline firing rate of 30 Hz.

When the stimulation frequency approached the baseline firing rate ($f_{stim} = 30$ Hz), the neuron rapidly entrained to the stimulus, also spiking with the same frequency (Time-series are shown in Figure C.3 in the appendix). When the stimulation frequency exceeded the baseline firing rate, the spike rate increased correspondingly. For $f_{stim} = 50$ Hz, the neuron's spike rate quickly rised to 50 Hz, paired with a rapid increase in entrainment (Figure C.4 in the appendix). At a higher stimulation frequency ($f_{stim} = 130$) Hz the spike rate gradually increased to a frequency lower than 130 Hz ($\approx$42 Hz) but the entrainment process was slower and showed fluctuations (Figure C.5 in the appendix). Overall, the regular spiking behaviour induced by the constant input is easily disturbed by the applied stimulation.

Introducing noise with $\sigma = 0.0125$ resulted in a baseline spike rate of 31.025 Hz. The results show the same trend as when $\sigma = 0$ and are visualized in the appendix (Figure C.7 in the appendix). When σ was doubled to 0.025, the initial PLV to the baseline spike rate dropped to zero (Figure C.8 in the appendix).

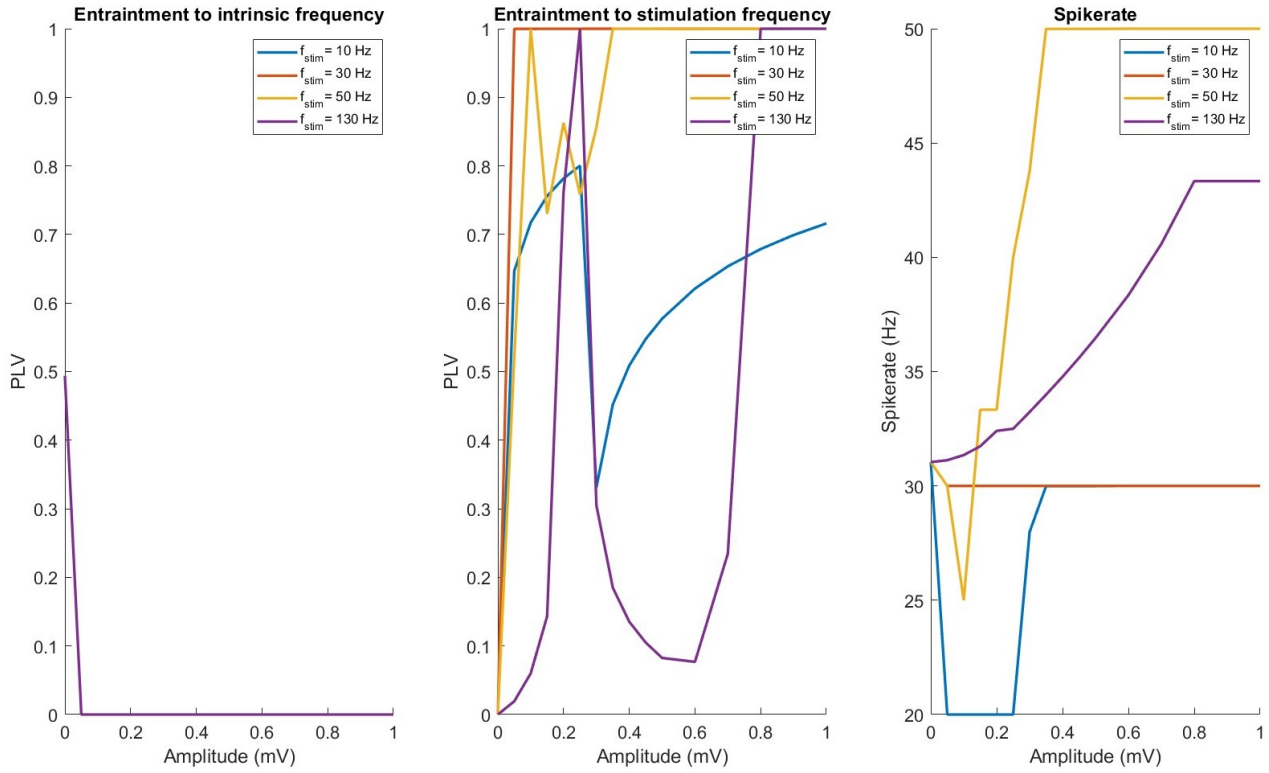

FIGURE 4.11: Entrainment and spike rate as a function of stimulation amplitude for the two-compartment model with a constant input $I_d = 77\mu A/cm^2$ and $\sigma = 0$ evaluated for different levels of stimulation frequencies (f_{stim}). Based on one simulation of one constant seed.

4.3.2 Exponential synaptic input results in similar (de)synchronization as the multi-compartment model

The synaptic input was changed to an exponential synaptic input, with noise, designed to achieve an initial entrainment to the intrinsic frequency of 11 Hz. This input resulted in a fluctuating resting membrane potential with irregular spikes (Figure 4.10b). In Figure 4.12 the PLV to the intrinsic frequency remained constant and the PLV to the stimulation frequency increased. The spike rate showed a small decrease from 0 to 3 mV and then started increasing rapidly. These trends are similar to the trends observed in the multi-compartment model (Figure 4.9).

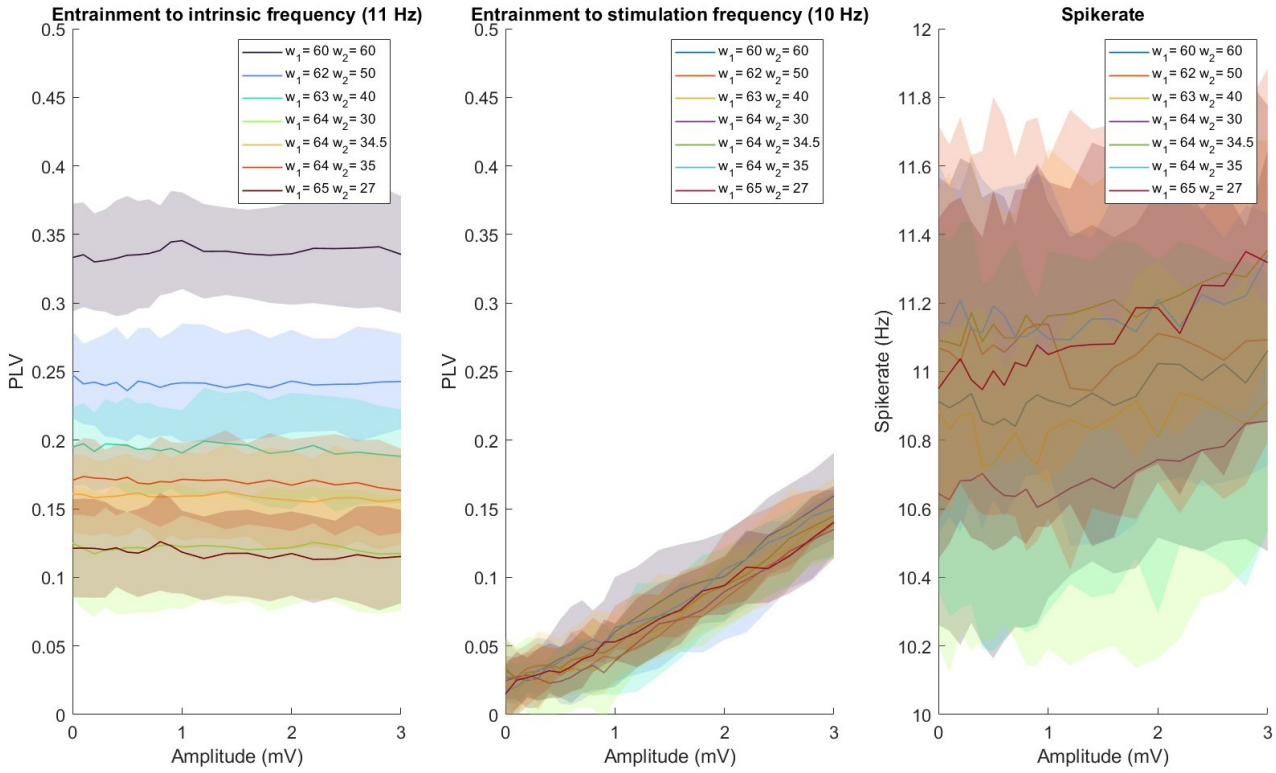

FIGURE 4.12: Entrainment and spike rate as a function of stimulation amplitude for the two-compartment model with two exponential synaptic inputs of 50 and 11 Hz. Stimulation frequency is kept constant at 10 Hz. Evaluated for different weights of both synapses (w_1 and w_2). Based on one simulation of 120 of six seeds. The line indicates the mean value across the seeds and the shade visualizes the standard deviation.

Chapter 5

Discussion

In this thesis, we explored the conditions under which neurons synchronize or desynchronize in response to an alternating weak electric field, using three different computational models. This study is motivated by the ongoing uncertainty regarding the mechanism of DBS [17, 19]. Various mechanisms [25] have been proposed in the literature, with most studies focusing on the direct and indirect effects of strong fields in the area close to where the electrode is implanted. However, there is a lack of research on the effects of weak electric fields further away. The success of non-invasive stimulation methods (i.e. tACS) suggests that weak fields could also have an impact. This study, therefore, focuses on exploring the impact of weak electric fields. Specifically, the effect of weak fields on the synchrony of neurons with respect to β frequencies (8-30 Hz) is investigated, since synchrony in the motor cortex plays an important role in the pathology of PD motor symptoms [11–13]. The hypothesis is that this pathology can be disrupted by DBS and that the weak electric fields play an important role in this by desynchronizing neurons in the motor cortex. Using computational models, the hypothesis that weak fields desynchronize neurons and strong field synchronize neurons has been tested. Three different models have been used: an oscillator model (SL model) and two single-cell models (two-compartment and multi-compartment).

Stuart-Landau model
The SL model showed that desynchronization can occur at high stimulation frequencies (>100 Hz), typically used in DBS. However, the whole (de)synchronization pattern did not only depend on the intrinsic and stimulation frequency but also on their ratio (Figure 4.4). One of the key limitations of the SL model is its phenomenological nature, as it does not incorporate physiological units or directly translate to biologically realistic settings. This limits the model's applicability to real-world scenarios. Despite this, the model's ability to replicate the findings of Krause et al. [27]—who validated their model against experimental results using tACS at 10 Hz—gives it some legitimacy for use in researching synchronization dynamics under specific conditions. However, its extrapolation to higher frequencies, such as those used in DBS, remains speculative.

A challenge in translating the model to biologically relevant settings is its representation of the amplitude. Because of the lack of physical units, the amplitude was expressed as a percentage of the ongoing oscillation amplitude. The stimulation amplitude did not exceed the amplitude of the ongoing oscillations. This approach was adopted by Krause et al. [27], because they investigated tACS and hippocampal neurons, which have membrane potential fluctuations of 1-2 mV at rest and tACS causes membrane fluctuations of 1 mV per V/m. However, this estimation may not apply to pyramidal neurons in the motor cortex, but their membrane fluctuations are not documented in the literature. Layer 2/3 pyramidal cells, however, showed resting membrane potential fluctuations up to 10 mV [49]. To address this limitation, a broader range of percentages should be explored.

Additionally, while the frequency parameters were assigned units for comparison with DBS stimulation frequencies, the other parameters remained unitless. This is done to compare it to stimulation frequencies used in DBS and since the time was defined in seconds by Krause et al. [27]. To ensure accuracy, we visually verified that 1 Hz corresponded to one oscillation per second in the time series data (e.g., Figure 4.1 where $f_{int} = 0.5$ Hz). Nevertheless, translating the intrinsic frequency into a biologically relevant parameter remains challenging. It represents the frequency of the ongoing oscillation, which Krause et al. [27] compared to the frequency neurons are most entrained to before stimulation. In this thesis, this frequency was increased to represent the pathological β frequencies. While the intrinsic frequency was set to a specific value, neurons entrain to a range of frequencies, rather than a single frequency. Therefore, to more accurately predict the effects of electrical stimulation, it would be necessary to average the outcomes over a spectrum of intrinsic frequencies, in the β range where pathological synchrony occurs.

The SL model showed that for higher stimulation frequencies as used in DBS, desynchronization could occur. And for an intrinsic frequency of 8 Hz, the higher stimulation frequencies resulted in the hypothesised pattern of weak field decreasing entrainment, and strong field increasing entrainment. However, the relationship between stimulation amplitude and (de)synchronization was very sensitive to variations in stimulation frequency, intrinsic frequency and their ratio. This sensitivity underscores the complexity of predicting neural responses to electrical stimulation, raising questions about the possibility of predicting (de)synchronization. This model is a first step in investigating the effects of higher stimulation frequencies on (de)synchronization, but more biologically realistic models are needed to draw stronger conclusions.

Multi-compartment model
The first step of using the multicompartment single-cell model from Tran et al. [29] was to reproduce the desynchronization effects they reported. [29]. We succeeded to partially replicate their findings (Figure 4.6). While we did observe a small desynchronization effect using the standard PLV method, this effect was not as pronounced as reported by Tran et al. One possible explanation for this is the sensitivity of the model to noise. Tran et al. performed their simulations across five different cell clones and averaged the results, whereas our simulations were conducted with only one clone (with two seeds). Variations in the seed value resulted in variations in the initial PLV and the magnitude of desynchronization, where the higher initial PLV resulted in the biggest desynchronization.

Thus, the observed lower magnitude of desynchronization in our study compared to Tran's results may be attributed to the variability introduced by the random seed and the absence of averaging across multiple cell clones. However, the desynchronization effect could not be found using the PPC method, which raises concerns about the reliability of the effect observed. The failure to replicate the desynchronization effect with the PPC method could suggest that the observed effect in their study was an artefact of the method used to calculate the PLV. While the PPC method was chosen to avoid sample size bias, the large number of spikes (over 1000) used in each calculation likely rules out sample size as the cause of the difference between the two metrics [41]. However, it is important to note that Vinck et al. [41] did not explore under what conditions the PLV can be reliably estimated from the square root of the PPC, especially for lower PLV and PPC values—precisely where the discrepancy between the methods occurred. Until the translation between these methods is better understood, it is advised to consider both methods.

Most of the simulations of the multi-compartment model used the sinusoidal waveform, to replicate the results from Tran et al. [29]. However, it is essential to test different waveforms, when investigating the

effect of the stimulation amplitude on desynchronization. Our findings suggest that sinusoidal waveforms are more effective in inducing neural entrainment than DBS waveforms. Both the DBS-positive and DBS-negative waveforms required a higher threshold for entraining (Figure 4.7), and activating the neuron (Figure 4.8). This implies that DBS waveforms with weak amplitudes may have a limited impact on synchronization. Nevertheless, it remains uncertain whether this limitation extends to desynchronization effects. The ability of the DBS-positive waveform to entrain the neuron at frequencies of 130 Hz with amplitudes of 30/40 V/m and the fact that the neuron can spike at high frequencies up to 150 Hz (Figure 4.8c) suggest that the model, in general, is suitable for studying high-frequency dynamics.

The direction of the DBS waveform also plays a critical role. The DBS-positive waveform exhibited a lower threshold for both spiking and entrainment compared to the DBS-negative waveform. With a positive pulse, the soma became more positive relative to the dendrite, leading to depolarization of the membrane and a lower threshold for action potential. In contrast, with the DBS-negative waveform, the negative pulse causes hyperpolarization of the soma, resulting in a higher threshold for action potentials.

In exploring whether increasing the initial PLV to an 11 Hz synaptic input would enhance desynchronization, our simulations did not support this hypothesis. Contrary to expectations, a higher initial PLV to the 11 Hz frequency, associated with pathological beta activity, did not lead to a decrease in PLV upon stimulation. This contrasts with Krause et al. [27], who observed desynchronization when the stimulation frequency was close to the intrinsic frequency.

A possible explanation for this is the way of implementing the pathological synaptic input. The pathological synaptic input provided by the second synapse in our model did not account for the effects of the stimulation on surrounding neurons. In the brain, electric fields affect a broader network of neurons, which can influence overall neural synchrony. The lack of interaction between the pathological input and the stimulation in our model suggests that the model is not suitable for studying the effects of electric fields on (de)synchronization.

The model's sensitivity to the weight and location of the synapse, as well as the seed for the noisy input, indicates the complexity of neural behaviours. The high sensitivity to these parameters underscores the challenge of using computational models to predict complex neural behaviour.

Ideally, future research focuses on developing biologically realistic models that incorporate interactions between the cause of the synchrony (in this case the synaptic input) and the effects of electric fields. Coupling multiple neurons together in a neural network is a possibility to do this. However, putting these realistic models in a network is computationally very expensive. Furthermore, it is uncertain whether incorporating multiple neurons with detailed morphology into the network provides additional useful information, compared to more simple neurons.

Two-compartment model

The primary motive for using this model was that it is computationally less demanding than the multi-compartment model. A constant dendritic input was used, which made the neuron spike at a specific spike rate. The input was in this case still unaffected by the electric field, but the frequency was determined through intrinsic properties, rather than the frequency of the input (as was the case for the second synapse of the multi-compartment model). The results showed that the entrainment to the baseline spike rate could easily be interrupted by external stimulation, so a desynchronization at this frequency. The decrease in entrainment to the baseline spike rate is due to an increase in entrainment

to the stimulation frequency, which means synchronization. However, the model is very susceptible to any input, whether that is noise or an electric field. The regular spiking behaviour induced by the constant input is unrealistic, and with the introduction of noise to simulate more natural behaviour, the initial PLV quickly goes to zero.

Moreover, the constant input resulted in a baseline spike rate of 31.05 Hz, which falls outside the beta range. This input level was chosen because only inputs with high precision (up to 8 decimal places) yielded lower spike rates in the beta range. When the input was too low, spiking was absent, due to a bifurcation where the limit cycle disappears if the stimulation amplitude is too low. An alternative approach involves applying input to the soma. It is also important to note that the model did not achieve spike rates above 55 Hz (Figure C.1), even with stimulation frequencies as high as 150 Hz. This raises questions about the model's suitability for studying high-frequency dynamics.

Subsequently, a more realistic synaptic input was tested, but the same problem as for the multi-compartment model occurred: the synaptic input did not incorporate any effects of the applied electric field, meaning it did not interact dynamically with the stimulation. The trend observed in this model is comparable to that observed in the multi-compartment model. However, this could be due to the implementation of the exponential synapse, which is equal in both models.

This model simplifies the complex morphology of a neuron, despite the findings in studies [30, 38, 39] that differences in morphologies affect neural responses to electric fields. These studies demonstrated that a lower morphologic parameter p increases a neuron's susceptibility to an electric field. In this thesis, p was fixed at 0.15, representing the asymmetrical structure of a pyramidal cell. However, with constant dendritic input, the neuron rapidly entrained to the stimulation, which is associated with a decreased entrainment to its intrinsic frequency (Figure 4.11). It would be interesting to investigate whether reducing p, leads to a slower entrainment to the stimulation and how this might affect the neuron's entrainment to its intrinsic frequency.

When using a constant input, it became apparent that bursts occur, in the sense that spikes are clustered together. We did not perform any burst-detecting analysis in this thesis, each spike is considered as a spike. However, for the constant dendritic input, the behaviour is very regular, making it possible to visually analyse this (see Figure C.2, C.3, C.4 and C.5 in the appendix). In the case of exponential synaptic input, more noise is present and the behaviour is not regular. However, bursting can still occur, which can affect the PLV. If individual spikes within bursts are classified as separate spikes, the PLV could appear reduced, even though the bursts themselves remain phase-locked, while the bursts are locked. Therefore it is recommended to include burst-detecting analysis.

Synchrony

One of the difficulties in analysing these models is how to specify synchrony. For the SL model, it was assumed that the amplitude of the oscillations of the oscillator represents how strongly the "neurons" are synchronized. For the single-cell models, we measure synchrony with entrainment to a specific frequency, based on Tran et al. [29] and Krause et al. [27] who calculated entrainment with respect to the stimulation frequency. Additionally, we also calculated entrainment with respect to an intrinsic frequency (determined by the synaptic input). The idea behind entrainment as a measure of synchrony is, that when single neurons are entrained to a specific frequency, they are synchronized to each other. Nevertheless, the synchrony within a neural population expands a wider range of frequencies.

In in-vivo experiments, Krause et al. [27] defined entrainment concerning the LFP, which captures a broad spectrum of frequencies but is susceptible to being dominated by the stimulation signal itself

during tACS. Similarly, Zhao et al. [28] used a network model of 1000 neurons and calculated the baseline PLV with respect to the LFP. During the stimulation, they calculated the PLV with respect to the tACS waveform. So, in both studies, the difference in entrainment may not only be due to the change of behaviour in the individual neuron but also to the appearance of the stimulation in the LFP. In the single-cell models, such an LFP is not defined. A solution could be to compute the PLV for many different frequencies, however this is computationally demanding. Therefore, it is recommended to use a measure of synchrony that is independent of frequency.

An entropy-based measure of synchrony [50] could be a solution. By quantifying the randomness of spike trains, entropy could provide a frequency-independent assessment of synchrony. This would allow for a more robust comparison of neural activity before and during stimulation, without the need to compute PLV across multiple frequencies. Future research on single-cell models should consider using a frequency-independent entrainment measure, such as entropy.

Future work
Given the limitations of the current models, drawing definitive conclusions about the hypothesis is challenging. The SL model shows desynchronization for specific parameter settings, however its underlying mechanism is poorly understood. The single-cell models show either no decrease in entrainment or an immediate decrease in entrainment to the intrinsic frequency because it entrains to the stimulation frequency. However, this decrease in entrainment is very unrealistic, since the model is very susceptible to any form of input. For these single-cell models, the key question is whether the absence of observed desynchronization is due to a lack of desynchronization itself or because the external input maintains synchrony. Future work should focus on incorporating the effect of electric fields into the pathological input to answer this question. One approach is to couple multiple neurons and use synchrony measures that calculate synchrony with respect to each other.

Zhao et al. [28] used a network model consisting of two-compartment conductance-based models and single-compartment interneurons to investigate the effects of tACS on synchrony. They showed promising results where low electric fields can decrease neural entrainment to the LFP, while high intensities enhance this entrainment. Similar to the single-cell models, this entrainment is used to measure the synchrony. This model provides a promising foundation for exploring similar effects in the context of DBS. However, their model is computationally expensive. A simpler approach is starting with two coupled neurons. Park et al. [51] demonstrated this by using two-compartment models to study the impact of direct current on synchrony between neurons. Although they used direct current, this method could serve as a basis for further exploration with alternating currents.

Incorporating the DBS waveform into these models is crucial, as weak fields ($<$3 V/m) with a DBS waveform do not seem to induce spiking or entrainment. This raises the question of whether desynchronization found in TACS studies with a sinusoidal waveform [27–29] will occur for a DBS waveform. Additionally, since the directionality of the DBS waveform influences neuronal responses, this factor should be taken into account. In single-cell models, both waveform types need to be considered, whereas in network models, varying the orientations of neurons could simulate the diverse orientations of neurons in cortical foldings.

Chapter 6

Conclusion

To address the question: "Under which conditions do neurons synchronize and desynchronize when there is an alternating weak electric field applied?", three different computational models have been investigated. The Stuart Landau model showed that desynchronization can occur at high stimulation frequencies, similar to those used in DBS. The hypothesis that weak fields desynchronize, while strong fields synchronize can be accepted under very specific parameter settings. However, the influence of these parameters (stimulation frequency, intrinsic frequency and its ratio) on the (de)synchronization pattern is poorly understood, limiting the conclusions that can be drawn from this model. The two single-cell models exhibited synchronization at the stimulation frequency, and only the two-compartment model with constant input showed desynchronization at a pathological β frequency. However, this desynchronization was very unrealistic due to the regular behaviour of the model and the susceptibility to noise. With the current results, we cannot confirm the hypothesis. However, the results highlight the critical role of synaptic input alterations induced by the electric field and suggest that single-cell models are insufficient to capture the dynamics of synchronization. This finding underscores the importance of coupling neurons together in a network model to investigate (de)synchronization properties. Consequently, further research, particularly involving network models, is necessary to definitively accept or reject the hypothesis.

Appendices

Appendix A

Stuard-Landau model

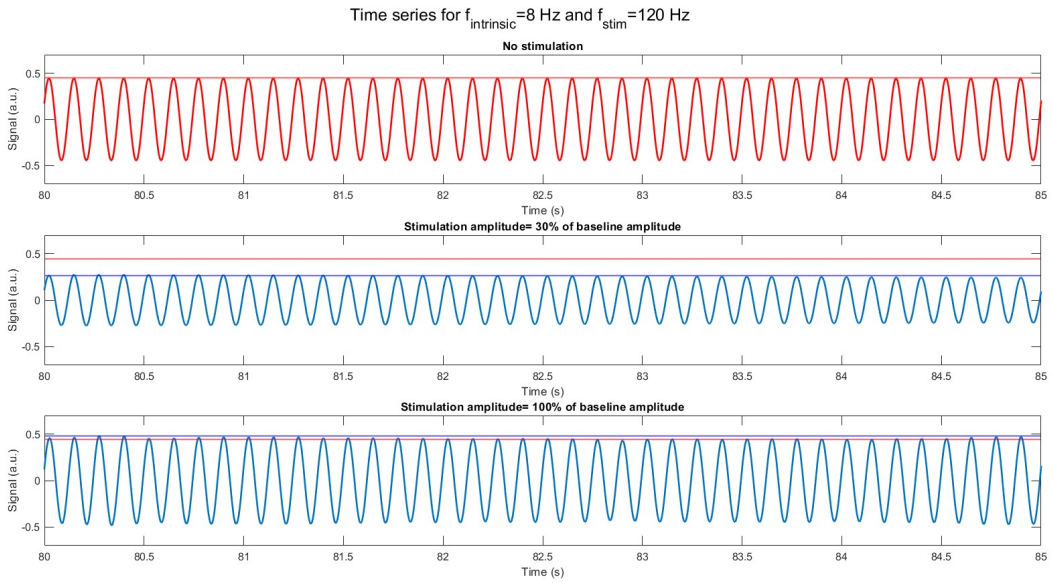

FIGURE A.1: Time series from Figure 4.3b, with $f_{stim} = 120$ Hz, $f_{intrinsic} = 8$ Hz, for the baseline condition (no stimulation) and a stimulation amplitude of 30% and 100% of the baseline amplitude. The red line represents the baseline amplitude, while the blue line indicates the amplitude for the corresponding condition. Amplitude is defined by the root-mean-squared value of the signal multiplied by $\sqrt{2}$.

Appendix B

Multi-compartment model

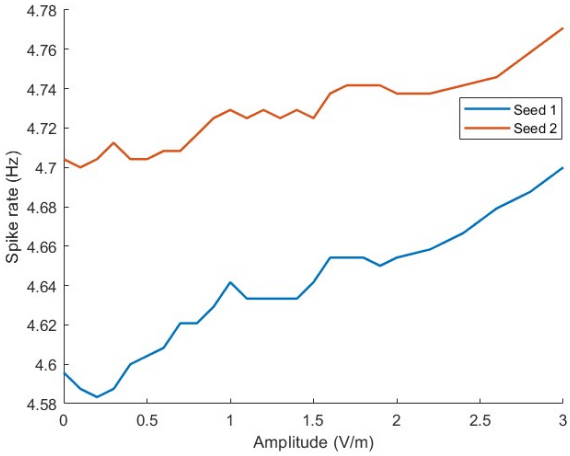

FIGURE B.1: Spike rate as a function of stimulation amplitude for the multi-compartment model with one synapse (w1 = 0.015). Stimulated with a sinusoidal waveform of 10 Hz. Based on simulations of 240 s, visualised for two different seeds.

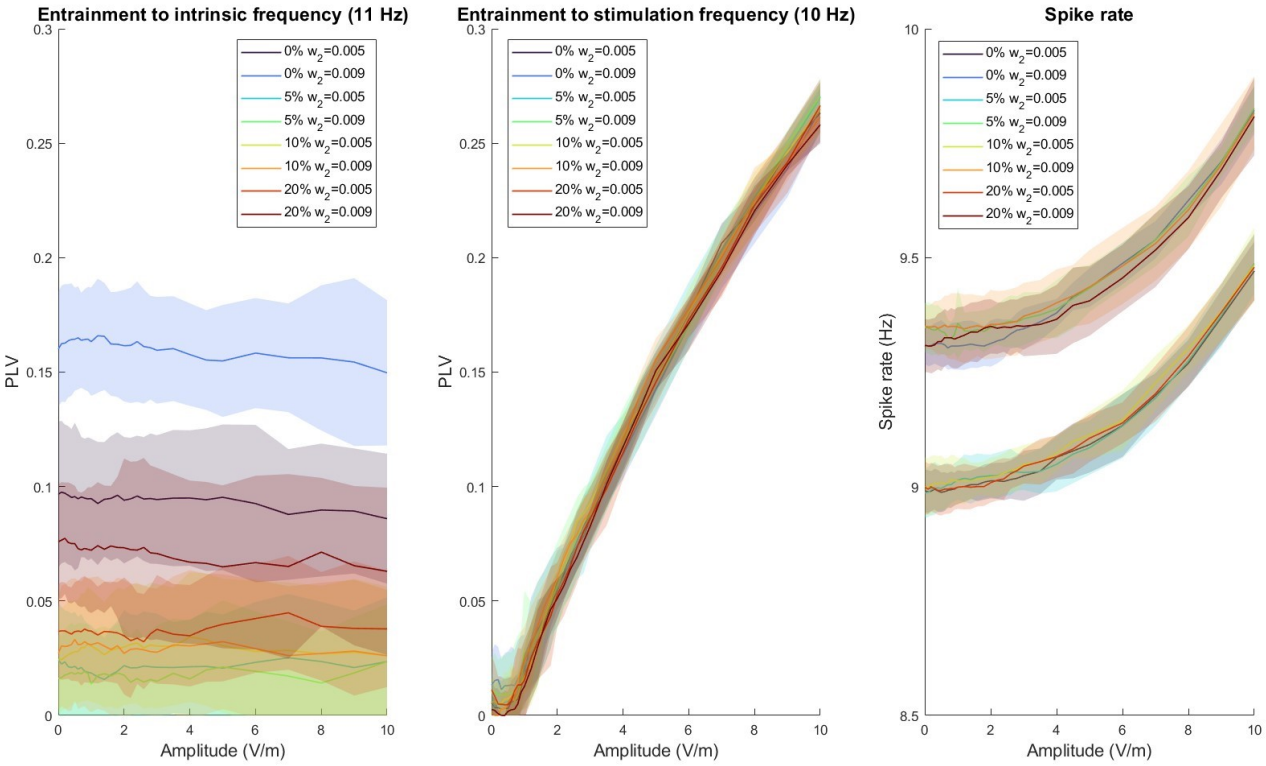

FIGURE B.2: Extension of Figure 4.9, for higher stimulation amplitudes. Entrainment and spike rate as a function of stimulation amplitude for the multi-compartment model with two synapses ($w_1 = 0.016$). The weight and jitter percentage of the second synapse is varied. Stimulated with a sinusoidal waveform of 10 Hz. Based on simulations of 120 s of six seeds. The line indicates the mean value across the seeds and the shade visualizes the standard deviation.

Appendix C

Two-compartment model

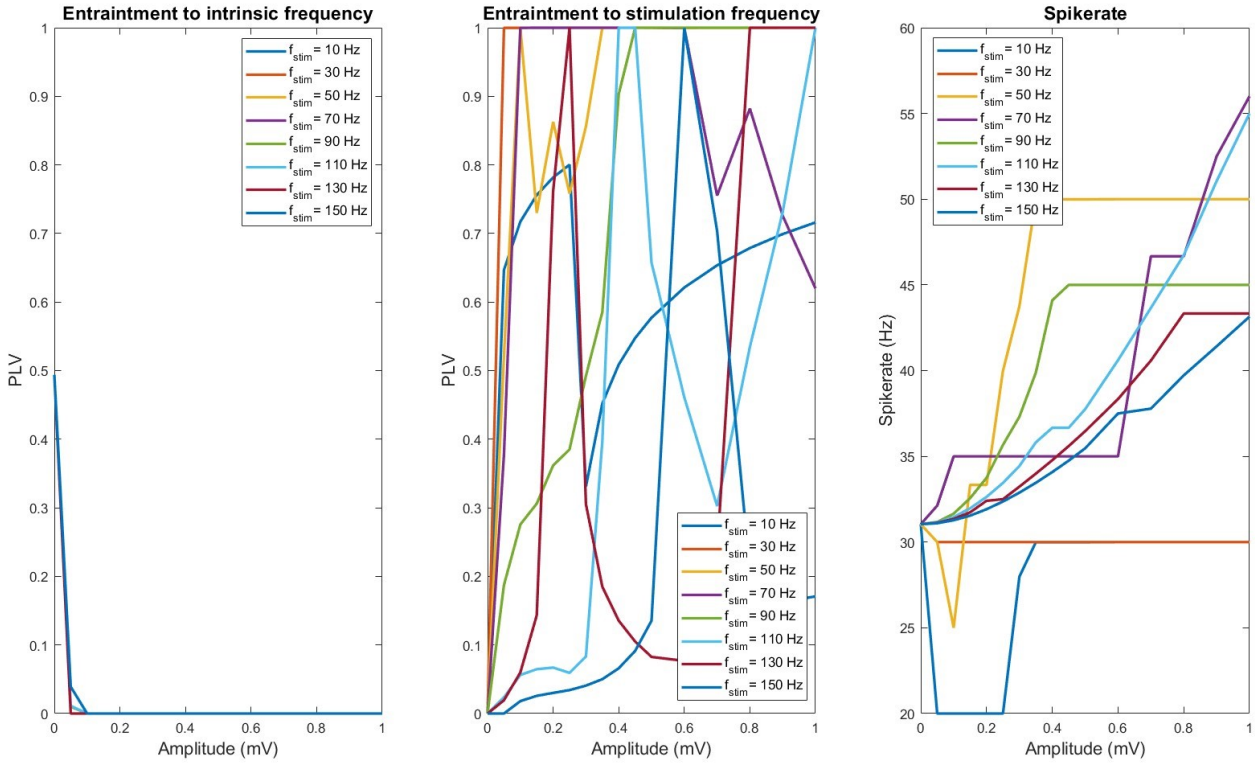

FIGURE C.1: Entrainment and spike rate as a function of stimulation amplitude for the two-compartment model with a constant input $I_d = 77\mu A/cm^2$ and $\sigma = 0$ evaluated for different levels of stimulation frequencies (f_{stim}). Based on simulation of 120 s.

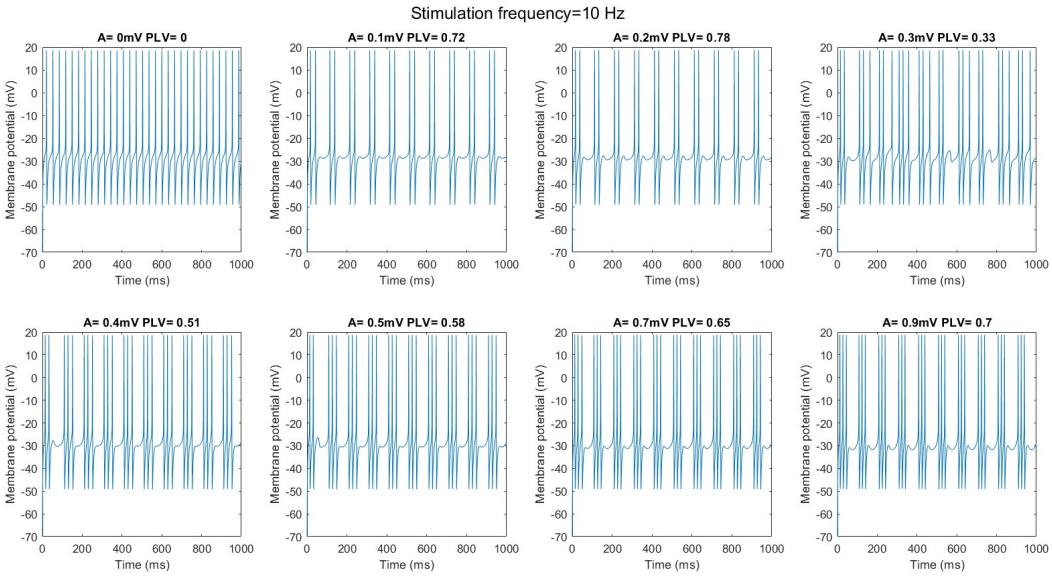

FIGURE C.2: Time series for the two-compartment model with constant input $I_d = 77\mu A/cm^2$ and $\sigma = 0$ for different stimulation amplitudes and $f_stim = 10$ Hz.

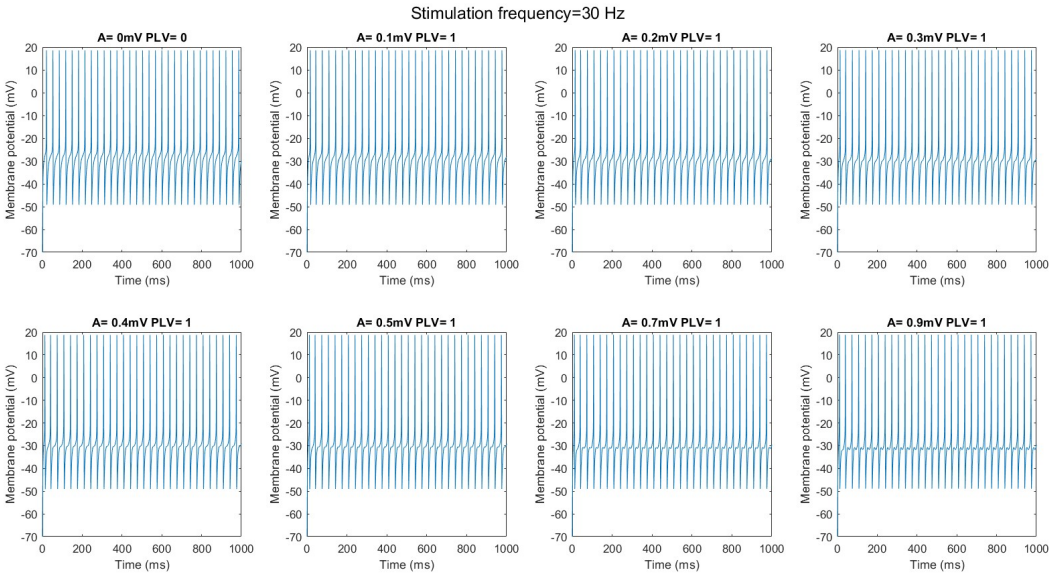

FIGURE C.3: Time series for the two-compartment model with constant input $I_d = 77\mu A/cm^2$ and $\sigma = 0$ for different stimulation amplitudes and $f_stim = 30$ Hz.

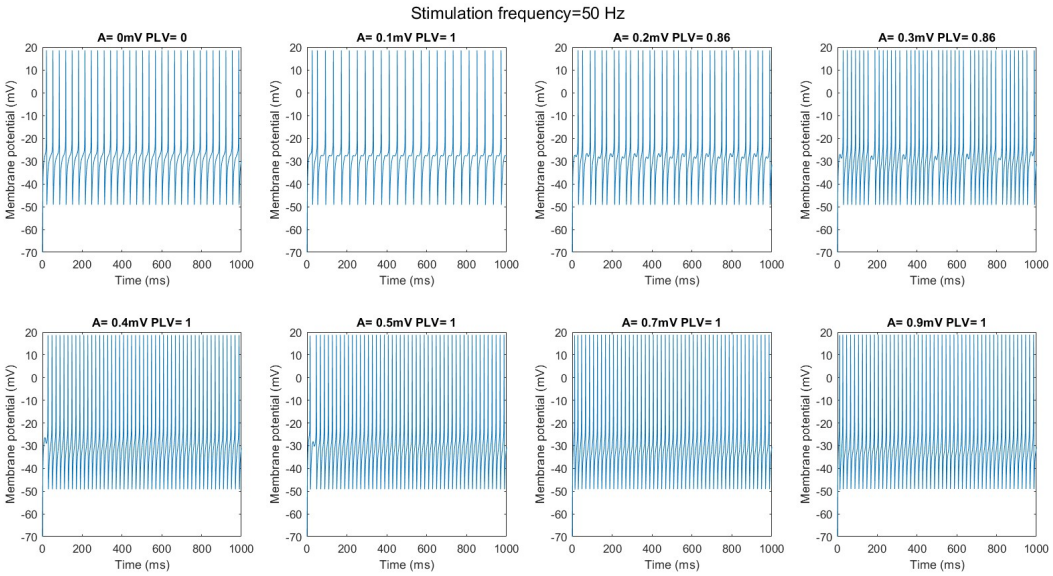

FIGURE C.4: Time series for the two-compartment model with constant input $I_d = 77\mu A/cm^2$ and $\sigma = 0$ for different stimulation amplitudes and $f_stim = 50$ Hz.

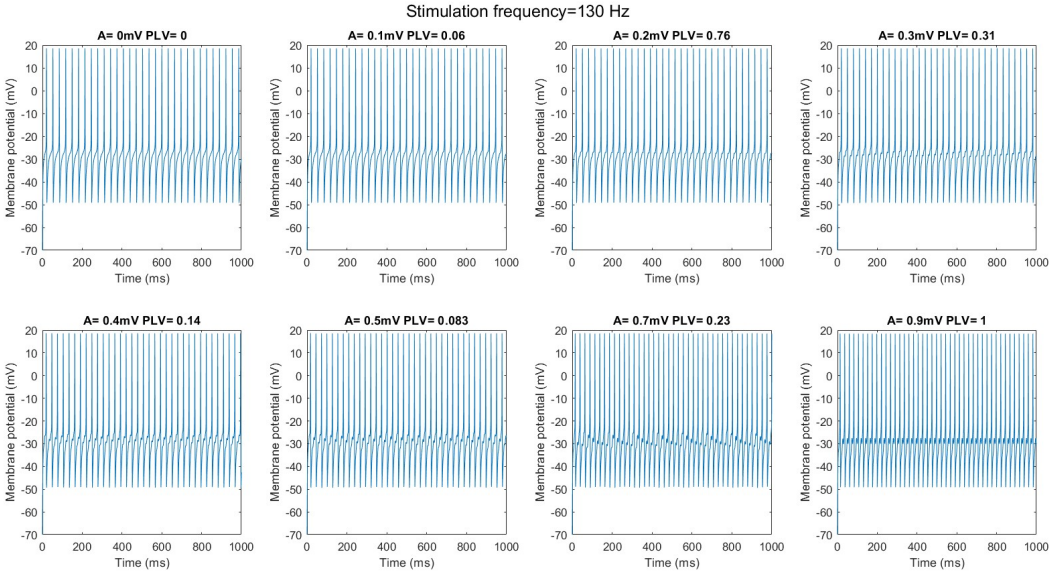

FIGURE C.5: Time series for the two-compartment model with constant input $I_d = 77\mu A/cm^2$ and $\sigma = 0$ for different stimulation amplitudes and $f_stim = 130$ Hz.

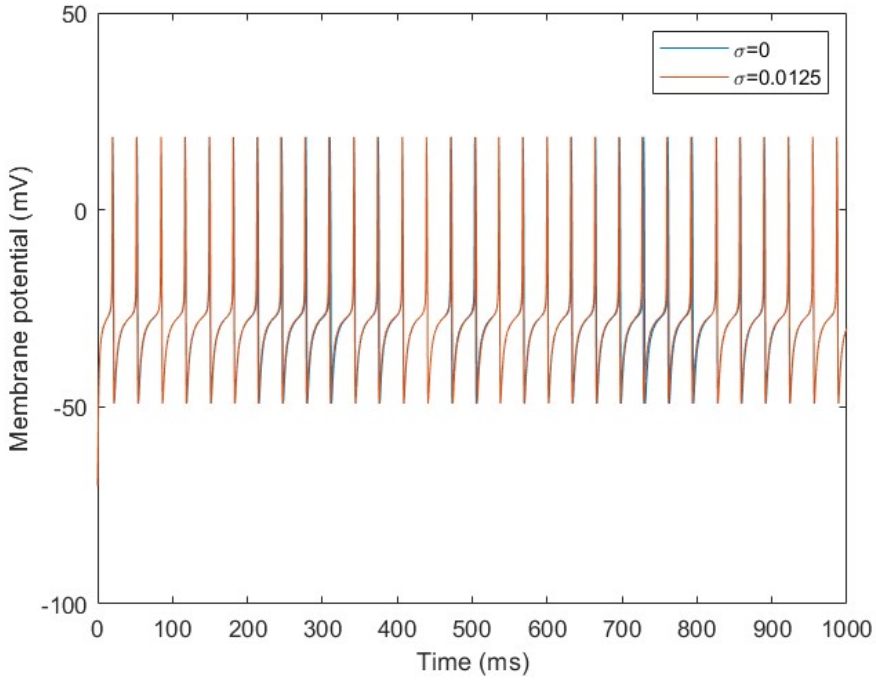

FIGURE C.6: Example of a time series of the two-compartment model with constant input for both $\sigma = 0$ and $\sigma = 0.0125$

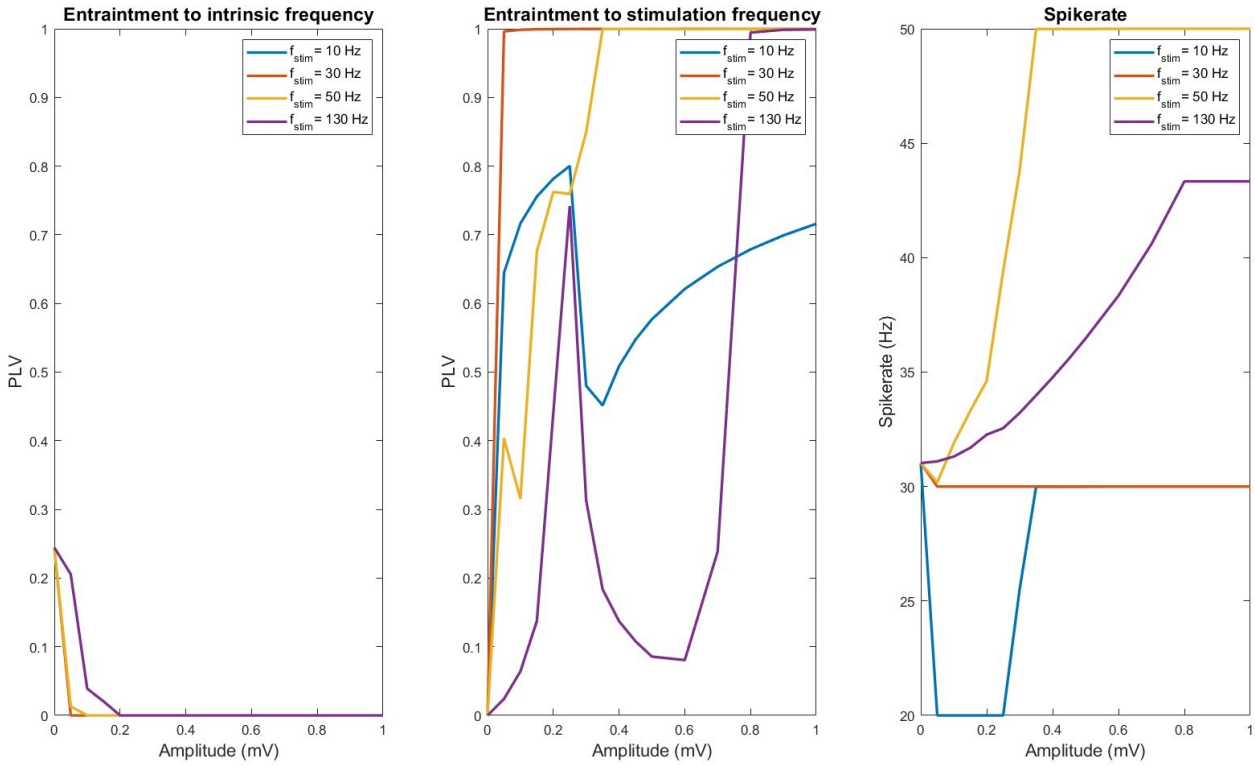

FIGURE C.7: Entrainment and spike rate as a function of stimulation amplitude for the two-compartment model with a constant input $I_d = 77\mu A/cm^2$ and $\sigma = 0.0125$ evaluated for different levels of stimulation frequencies (f_{stim}). Based on one simulation of 120 s of one constant seed.

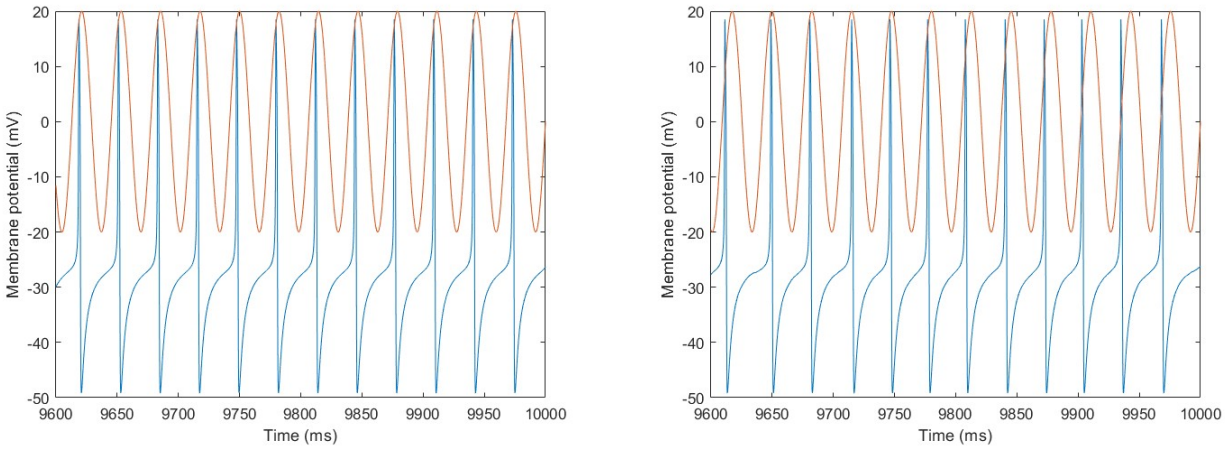

(A) $\sigma = 0.0$ (B) $\sigma = 0.025$

FIGURE C.8: Example of a time series of the two-compartment model with constant input and two values of σ. Blue indicates the membrane potential of the neuron, orange indicates a sinusoidal with the same frequency as the spike rate of the neuron. The figure shows that due to the addition of noise, the spike times are not consistent with the sinusoidal waveform.

Bibliography

1. Kalia, L. V. & Lang, A. E. Parkinson's disease. *The Lancet* **386,** 896–912. ISSN: 0140-6736. doi:10.1016/S0140-6736(14)61393-3 (Aug. 2015).
2. Wichmann, T. & DeLong, M. R. Deep Brain Stimulation for Movement Disorders of Basal Ganglia Origin: Restoring Function or Functionality? *Neurotherapeutics* **13,** 264. ISSN: 18787479. doi:10.1007/S13311-016-0426-6. /pmc/articles/PMC4824026//pmc/articles/PMC4824026/?report=abstracthttps://www.ncbi.nlm.nih.gov/pmc/articles/PMC4824026/ (Apr. 2016).
3. Underwood, C. F. & Parr-Brownlie, L. C. Primary motor cortex in Parkinson's disease: Functional changes and opportunities for neurostimulation. *Neurobiology of Disease* **147,** 105159. ISSN: 0969-9961. doi:10.1016/J.NBD.2020.105159 (Jan. 2021).
4. Rubchinsky, L. L., Park, C. & Worth, R. M. Intermittent neural synchronization in Parkinson's disease. *Nonlinear Dynamics* **68,** 329–346. ISSN: 1573-269X. doi:10.1007/s11071-011-0223-z. https://doi.org/10.1007/s11071-011-0223-z (2012).
5. Ashkan, K., Rogers, P., Bergman, H. & Ughratdar, I. Insights into the mechanisms of deep brain stimulation. *Nature Reviews Neurology 2017 13:9* **13,** 548–554. ISSN: 1759-4766. doi:10.1038/nrneurol.2017.105. https://www.nature.com/articles/nrneurol.2017.105 (July 2017).
6. James Surmeier, D., Obeso, J. A. & Halliday, G. M. Parkinson's Disease Is Not Simply a Prion Disorder. *Journal of Neuroscience* **37,** 9799–9807. ISSN: 0270-6474. doi:10.1523/JNEUROSCI.1787-16.2017. https://www.jneurosci.org/content/37/41/9799https://www.jneurosci.org/content/37/41/9799.abstract (Oct. 2017).
7. Bergman, H. *et al.* Physiological aspects of information processing in the basal ganglia of normal and parkinsonian primates. *Trends in Neurosciences* **21,** 32–38. ISSN: 0166-2236. doi:10.1016/S0166-2236(97)01151-X (Jan. 1998).
8. Hammond, C., Bergman, H. & Brown, P. Pathological synchronization in Parkinson's disease: networks, models and treatments. *Trends in Neurosciences* **30,** 357–364. ISSN: 0166-2236. doi:10.1016/J.TINS.2007.05.004 (July 2007).
9. Brown, P. & Williams, D. Basal ganglia local field potential activity: Character and functional significance in the human. *Clinical Neurophysiology* **116,** 2510–2519. ISSN: 1388-2457. doi:10.1016/J.CLINPH.2005.05.009 (Nov. 2005).
10. Feng, H. *et al.* Characteristics of subthalamic oscillatory activity in parkinsonian akinetic-rigid type and mixed type. *International Journal of Neuroscience* **126,** 819–828. ISSN: 15635279. doi:10.3109/00207454.2015.1074225. https://www.tandfonline.com/doi/abs/10.3109/00207454.2015.1074225 (Sept. 2016).
11. Goldberg, J. A. *et al.* Enhanced Synchrony among Primary Motor Cortex Neurons in the 1-Methyl-4-Phenyl-1,2,3,6-Tetrahydropyridine Primate Model of Parkinson's Disease. *Journal of Neuroscience* **22,** 4639–4653. ISSN: 0270-6474. doi:10.1523/JNEUROSCI.22-11-04639.2002. https://www.jneurosci.org/content/22/11/4639https://www.jneurosci.org/content/22/11/4639.abstract (June 2002).

12. Pasquereau, B. & Turner, R. S. Primary Motor Cortex of the Parkinsonian Monkey: Differential Effects on the Spontaneous Activity of Pyramidal Tract-Type Neurons. *Cerebral Cortex (New York, NY)* **21,** 1362. ISSN: 10473211. doi:10.1093/CERCOR/BHQ217. /pmc/articles/PMC3097989/ /pmc/articles/PMC3097989/?report=abstracthttps://www.ncbi.nlm.nih.gov/pmc/articles/PMC3097989/ (June 2011).

13. Gatev, P., Darbin, O. & Wichmann, T. Oscillations in the basal ganglia under normal conditions and in movement disorders. *Movement Disorders* **21,** 1566–1577. ISSN: 1531-8257. doi:10.1002/MDS.21033. https://onlinelibrary.wiley.com/doi/full/10.1002/mds.21033https://onlinelibrary.wiley.com/doi/abs/10.1002/mds.21033https://movementdisorders.onlinelibrary.wiley.com/doi/10.1002/mds.21033 (Oct. 2006).

14. Brown, P. Abnormal oscillatory synchronisation in the motor system leads to impaired movement. *Current Opinion in Neurobiology* **17,** 656–664. ISSN: 0959-4388. doi:10.1016/J.CONB.2007.12.001 (Dec. 2007).

15. Macphee, G. *Diagnosis and differential diagnosis of Parkinson's disease* 41–75. ISBN: 9781498791007. doi:10.1201/9781315365428-4 (2018).

16. Neumann, W. J., Steiner, L. A. & Milosevic, L. Neurophysiological mechanisms of deep brain stimulation across spatiotemporal resolutions. *Brain* **146,** 4456. ISSN: 14602156. doi:10.1093/BRAIN/AWAD239. /pmc/articles/PMC10629774//pmc/articles/PMC10629774/?report=abstracthttps://www-ncbi-nlm-nih-gov.ezproxy2.utwente.nl/pmc/articles/PMC10629774/ (Nov. 2023).

17. Volkmann, J. Deep brain stimulation for the treatment of Parkinson's disease. *Journal of clinical neurophysiology : official publication of the American Electroencephalographic Society* **21,** 6–17. ISSN: 0736-0258. doi:10.1097/00004691-200401000-00003. https://pubmed.ncbi.nlm.nih.gov/15097290/ (2004).

18. Deuschl, G. *et al.* A Randomized Trial of Deep-Brain Stimulation for Parkinson's Disease. *https://doi.org/10.10* **355,** 896–908. ISSN: 0028-4793. doi:10.1056/NEJMOA060281. https://www.nejm.org/doi/10.1056/NEJMoa060281 (Aug. 2006).

19. Benabid, A. L., Chabardes, S., Mitrofanis, J. & Pollak, P. Deep brain stimulation of the subthalamic nucleus for the treatment of Parkinson's disease. *The Lancet Neurology* **8,** 67–81. ISSN: 1474-4422. doi:https://doi.org/10.1016/S1474-4422(08)70291-6. https://www.sciencedirect.com/science/article/pii/S1474442208702916 (2009).

20. Perlmutter, J. S. & Mink, J. W. DEEP BRAIN STIMULATION. *https://doi.org/10.1146/annurev.neuro.29.05* **29,** 229–257. ISSN: 0147006X. doi:10.1146/ANNUREV.NEURO.29.051605.112824. https://www.annualreviews.org/doi/abs/10.1146/annurev.neuro.29.051605.112824 (June 2006).

21. Parsons, T. D., Rogers, S. A., Braaten, A. J., Woods, S. P. & Tröster, A. I. Cognitive sequelae of subthalamic nucleus deep brain stimulation in Parkinson's disease: a meta-analysis. *The Lancet Neurology* **5,** 578–588. ISSN: 1474-4422. doi:10.1016/S1474-4422(06)70475-6 (July 2006).

22. Zarzycki, M. Z. & Domitrz, I. Stimulation-induced side effects after deep brain stimulation – a systematic review. *Acta Neuropsychiatrica* **32,** 57–64. ISSN: 0924-2708. doi:DOI:10.1017/neu.2019.35. https://www.cambridge.org/core/product/01078271B9C688C2FC72961436757D1C (2020).

23. McIntyre, C. C. & Hahn, P. J. Network perspectives on the mechanisms of deep brain stimulation. *Neurobiology of Disease* **38,** 329–337. ISSN: 0969-9961. doi:10.1016/J.NBD.2009.09.022 (June 2010).

24. Li, Q., Qian, Z. M., Arbuthnott, G. W., Ke, Y. & Yung, W. H. Cortical Effects of Deep Brain Stimulation: Implications for Pathogenesis and Treatment of Parkinson Disease. *JAMA Neurology* **71,** 100–103. ISSN: 2168-6149. doi:10.1001/JAMANEUROL.2013.4221. https://jamanetwork.com/journals/jamaneurology/fullarticle/1763959 (Jan. 2014).

25. Schor, J. S. *et al.* Therapeutic deep brain stimulation disrupts movement-related subthalamic nucleus activity in parkinsonian mice. *eLife* **11** (eds Ding, J., Huguenard, J. R. & Jaeger, D.) e75253. ISSN: 2050-084X. doi:10.7554/eLife.75253. https://doi.org/10.7554/eLife.75253 (2022).

26. Wilson, C., Beverlin, B. & Netoff, T. *Chaotic Desynchronization as the Therapeutic Mechanism of Deep Brain Stimulation* 2011. https://www.frontiersin.org/articles/10.3389/fnsys.2011.00050.

27. Krause, M. R., Vieira, P. G., Thivierge, J.-P. & Pack, C. C. Brain stimulation competes with ongoing oscillations for control of spike timing in the primate brain. *PLOS Biology* **20,** e3001650. https://doi.org/10.1371/journal.pbio.3001650 (May 2022).

28. Zhao, Z., Shirinpour, S., Tran, H., Wischnewski, M. & Opitz, A. Intensity- and frequency-specific effects of transcranial alternating current stimulation are explained by network dynamics. *Journal of Neural Engineering* **21,** 026024. ISSN: 1741-2552. doi:10.1088/1741-2552/AD37D9. https://iopscience.iop.org/article/10.1088/1741-2552/ad37d9https://iopscience.iop.org/article/10.1088/1741-2552/ad37d9/meta (Apr. 2024).

29. Tran, H., Shirinpour, S. & Opitz, A. Effects of transcranial alternating current stimulation on spiking activity in computational models of single neocortical neurons. *NeuroImage* **250,** 118953. doi:10.1016/j.neuroimage.2022.118953. https://app.dimensions.ai/details/publication/pub.1145098560https://doi.org/10.1016/j.neuroimage.2022.118953 (Nov. 2022).

30. Wei, X., Yin, X., Lu, M., Yi, G. & Wang, J. Dependence of sinusoidal electric field effect on neuronal morphological properties. *International Journal of Modern Physics B* **29.** ISSN: 17936578. doi:10.1142/S0217979215500927 (2015).

31. Ladenbauer, J. & Obermayer, K. Weak electric fields promote resonance in neuronal spiking activity: Analytical results from two-compartment cell and network models. *PLOS Computational Biology* **15,** e1006974. https://doi.org/10.1371/journal.pcbi.1006974 (Apr. 2019).

32. Hines, M. L. & Carnevale, N. T. The NEURON Simulation Environment. *Neural Computation* **9,** 1179–1209. ISSN: 0899-7667. doi:10.1162/neco.1997.9.6.1179. https://doi.org/10.1162/neco.1997.9.6.1179 (Aug. 1997).

33. Halavi, M., Hamilton, K., Parekh, R. & Ascoli, G. *Digital Reconstructions of Neuronal Morphology: Three Decades of Research Trends* 2012. https://www.frontiersin.org/articles/10.3389/fnins.2012.00049.

34. Markram, H. *et al.* Reconstruction and Simulation of Neocortical Microcircuitry. *Cell* **163,** 456–492. ISSN: 0092-8674. doi:10.1016/j.cell.2015.09.029. https://doi.org/10.1016/j.cell.2015.09.029 (Oct. 2015).

35. Ramaswamy, S. *et al. The neocortical microcircuit collaboration portal: a resource for rat somatosensory cortex* 2015. https://www.frontiersin.org/articles/10.3389/fncir.2015.00044.

36. Druckmann, S. *et al.* A novel multiple objective optimization framework for constraining conductance-based neuron models by experimental data. www.frontiersin.org (2007).

37. Aberra, A. S., Peterchev, A. V. & Grill, W. M. Biophysically realistic neuron models for simulation of cortical stimulation. *Journal of Neural Engineering* **15,** 66023. ISSN: 1741-2552. doi:10.1088/1741-2552/aadbb1. https://dx.doi.org/10.1088/1741-2552/aadbb1 (2018).

38. Yi, G.-S. *et al.* Exploring action potential initiation in neurons exposed to DC electric fields through dynamical analysis of conductance-based model. *Communications in Nonlinear Science and Numerical Simulation* **19,** 1474–1485. ISSN: 1007-5704. doi:https://doi.org/10.1016/j.cnsns.2013.09.026. https://www.sciencedirect.com/science/article/pii/S1007570413004267 (2014).

39. Yi, G.-S. *et al.* Neuronal Spike Initiation Modulated by Extracellular Electric Fields. *PLoS ONE* **9,** 97481. doi:10.1371/journal.pone.0097481 (2014).

40. Yi, G.-S. *et al.* Exploring how extracellular electric field modulates neuron activity through dynamical analysis of a two-compartment neuron model. doi:10.1007/s10827-013-0479-z (2014).

41. Vinck, M., van Wingerden, M., Womelsdorf, T., Fries, P. & Pennartz, C. M. A. The pairwise phase consistency: A bias-free measure of rhythmic neuronal synchronization. *NeuroImage* **51,** 112–122. ISSN: 1053-8119. doi:https://doi.org/10.1016/j.neuroimage.2010.01.073. https://www.sciencedirect.com/science/article/pii/S1053811910000959 (2010).

42. Doelling, K. B. & Assaneo, M. F. Neural oscillations are a start toward understanding brain activity rather than the end. *PLOS Biology* **19,** e3001234. https://doi.org/10.1371/journal.pbio.3001234 (May 2021).

43. Radman, T., Ramos, R. L., Brumberg, J. C. & Bikson, M. Role of cortical cell type and morphology in subthreshold and suprathreshold uniform electric field stimulation in vitro. *Brain Stimulation* **2,** 215–228. ISSN: 1935-861X. doi:https://doi.org/10.1016/j.brs.2009.03.007. https://www.sciencedirect.com/science/article/pii/S1935861X09000424 (2009).

44. Lempka, S. F., Howell, B., Gunalan, K., Machado, A. G. & McIntyre, C. C. Characterization of the stimulus waveforms generated by implantable pulse generators for deep brain stimulation. *Clinical Neurophysiology* **129,** 731–742. ISSN: 1388-2457. doi:https://doi.org/10.1016/j.clinph.2018.01.015. https://www.sciencedirect.com/science/article/pii/S1388245718300300 (2018).

45. Foutz, T. J. & McIntyre, C. C. Evaluation of novel stimulus waveforms for deep brain stimulation. *Journal of Neural Engineering* **7,** 66008. ISSN: 1741-2552. doi:10.1088/1741-2560/7/6/066008. https://dx.doi.org/10.1088/1741-2560/7/6/066008 (2010).

46. Vieira, P. G., Krause, M. R. & Pack, C. C. tACS entrains neural activity while somatosensory input is blocked. *PLOS Biology* **18,** e3000834. https://doi.org/10.1371/journal.pbio.3000834 (Oct. 2020).

47. Haggie, L., Besier, T. & McMorland, A. J. Modelling Spontaneous Firing Activity of the Motor Cortex in a Spiking Neural Network with Random and Local Connectivity. *Neurons, Behavior, Data analysis, and Theory,* 1–22. doi:10.51628/001c.82127 (2023).

48. Mohan, H. *et al.* Dendritic and Axonal Architecture of Individual Pyramidal Neurons across Layers of Adult Human Neocortex. *Cerebral Cortex* **25,** 4839–4853. ISSN: 1047-3211. doi:10.1093/cercor/bhv188. https://doi.org/10.1093/cercor/bhv188 (Dec. 2015).

49. Fernandez, F. R., Noueihed, J. & White, J. A. Voltage-Dependent Membrane Properties Shape the Size But Not the Frequency Content of Spontaneous Voltage Fluctuations in Layer 2/3 Somatosensory Cortex. *The Journal of Neuroscience* **39,** 2221 LP –2237. doi:10.1523/JNEUROSCI.1648-18.2019. http://www.jneurosci.org/content/39/12/2221.abstract (Mar. 2019).

50. Kajikawa, Y. & Hackett, T. A. Entropy analysis of neuronal spike train synchrony. *Journal of Neuroscience Methods* **149,** 90–93. ISSN: 0165-0270. doi:https://doi.org/10.1016/j.jneumeth.2005.05.011. https://www.sciencedirect.com/science/article/pii/S0165027005001433 (2005).

51. Park, E.-H., Barreto, E., Gluckman, B. J., Schiff, S. J. & So, P. A Model of the Effects of Applied Electric Fields on Neuronal Synchronization. *Journal of Computational Neuroscience* **19,** 53–70. ISSN: 1573-6873. doi:10.1007/s10827-005-0214-5. https://doi.org/10.1007/s10827-005-0214-5 (2005).